Reynolds-Averaged Two-Fluid Model prediction of moderately dilute fluid-particle flow over a backward-facing step

M. Riella*, R. Kahraman, G.R. Tabor

College of Engineering, Mathematics and Physical Sciences, University of Exeter, North Park Road, Exeter EX4 4QF, UK

Abstract

In this work a Reynolds-Averaged two-fluid fully coupled model (RA-TFM) for modelling of turbulent fluid-particle flow is implemented in OpenFOAM and applied to a vertically orientated backward-facing step. Three particle classes with varying mass loadings (10-40%) and different Stokes number are investigated. Details of the implementation and solution procedure are provided with special attention given to challenging terms. The prediction of mean flow statistics are in good agreement with the data from literature and show a distinct improvement over current model predictions. This improvement was due to the separation of the particle turbulent kinetic energy k_p, and the granular temperature Θ_p, in which the large scale correlated motion and small scale uncorrelated motion are governed by separate transport equations. For each case simulated in this work, turbulence attenuation was accurately predicted, a finding that is attributed to separate coupling terms in both transport equations of k_p and ε_p.

Keywords: `Turbulence attenuation`, `Backward-facing step`, `RA-TFM`, `OpenFOAM`

*Corresponding author

Email address: `mjr214@exeter.ac.uk` (M. Riella)

1. Introduction

Modulation of turbulence is a complex two-way coupled phenomenon [14] and can be caused by fluid-particle interaction and/or particle-wall interaction. Modulation can result in an increase in the fluid-phase fluctuating velocities [24] due to particle vortex shedding [40], which is caused by a large particle Reynolds number, Re_p. Conversely, modulation of turbulence can result in the reduction of fluid-phase fluctuating velocities, i.e. attenuation. This behaviour is prevalent in fluid-particle flows due to high density ratios ($\rho_p \gg \rho_f$). This leads to the mean-feedback effect through drag - their primary coupling mechanism. Turbulence attenuation as a result of small heavy particles in the carrier flow is well established in the literature [15, 24, 26, 33, 50, 54, 57] and has been shown to be further influenced by the inhomogeneity of wall-bounded flow [53].

To date there have been numerous experimental studies investigating small heavy particles in wall-bounded, high Reynolds number flow [4, 9, 33, 50]. One valuable study is that of Fessler and Eaton [19] in which mean and turbulence statistics of dilute [14] fluid-particle flow were recorded in a vertically orientated backward-facing step. They report turbulence attenuation across three particle classifications (different Stokes number and mass loadings) and provide valuable insights into the particle behaviour in the free shear layer. Traditionally, the backward-facing step has been used as a benchmark for validation of single-phase turbulence models, as flow separation, reattachment and redevelopment are rife in engineering applications. Due to the complex nature of turbulence attenuation and the challenging physics in a backward-facing step configuration, its successful prediction has proven difficult [10, 36, 38, 51, 58].

There are two main approaches for predicting macroscale fluid-particle systems: the Eulerian-Lagrangian (E-L) method in which the fluid-phase is solved in an Eulerian frame and the particle-phase is solved with Lagrangian equations. Typically, all scales of motion are resolved except the boundary layers on the particle surfaces resulting in a high resolution of the flow field. It follows that E-L simulations are used for understanding fundamental phenomenon e.g. clustering [6, 49], and verifying experimental observations [25, 34]. Due to their expensive cost as each particle requires its own momentum equation, large particulate systems with high Reynolds number become inviable. This leads to the second approach: the Eulerian-Eulerian (E-E) methodology models both the fluid- and particle-phase as interpenetrating continua resulting in both phases acting as "fluids". This reduces the computational cost considerably with the fully resolved scales of E-L being modelled. This approach then relies on constitutive relations to close the governing equations.

Numerous two-fluid (E-E) models have been derived using a one-step averaging

process [1, 13, 28, 47] e.g. volume- or time-averaging. Within this methodology, kinetic theory is used to close the particle-phase stress that appears in its momentum equation. This approach has been applied by many authors [2, 11, 12, 16, 27, 40, 52, 60] with varying degrees of success. Recently, Fox [21] has shown that a two-step process is required in order to derive a Reynolds-Averaged multiphase turbulence model. In the aforementioned models, the multiphase models are derived analogously to a single-phase model using time- or volume-averaging techniques that can lead to ill-formed equations e.g. time averaging results in a diffusive term in the continuity equation.

In addition to this, a conceptual error has been highlighted. The statement $k_p = 3\langle\Theta\rangle_p$ is often found in these models which is inaccurate. This is due to the particle turbulent kinetic energy k_p, and the phase averaged (PA) granular temperature $\langle\Theta\rangle_p$, belonging to two different realisations of the flow. This distinction was first highlighted by Février et al. [20] in which particle velocities are decomposed into correlated k_p large-scale motion and uncorrelated $\langle\Theta\rangle_p$ small-scale motion. Both quantities are a result of separate models. It was shown that the correlated motion k_p arises due to the hydrodynamic (macroscale) model and the uncorrelated motion $\langle\Theta\rangle_p$ arises due to the kinetic (mesoscale) model.

The two-step derivation of Fox [21] has been shown to circumvent these issues. Beginning at the kinetic (mesoscale) equation [22], phase-space integration is applied to find the hydrodynamic (macroscale) moment equation which is then Reynolds-Averaged to form the Reynolds-Averaged Two-Fluid model (RA-TFM) after the appropriate closure modelling has been applied. This approach results in separate transport equations for the particle turbulence kinetic energy k_p and the PA granular temperature $\langle\Theta\rangle_p$. Through the derivation of k_p the particle turbulent kinetic energy dissipation ε_p, is defined which appears as a source term in the transport equation of the PA granular temperature, $\langle\Theta\rangle_p$. This cascade of energy from correlated motion to uncorrelated motion is a crucial distinction. This leads to the particle fluctuation energy being written as $\kappa_p = k_p + 1.5\langle\Theta\rangle_p$. Février et al. [20] found that even for non-collisional flow, separate transport equations for k_p and $\langle\Theta\rangle_p$ were essential, a direct result of the energy cascade outlined previously. Given these recent advances in the field, the modelling of previously challenging turbulent fluid-particle interactions in the Eulerian-Eulerian framework become clearer and their successful prediction more likely.

The overarching motivation of the present work is to increase the current understanding of the modelling of turbulent fluid-particle interaction in a complex flow field. We confine ourselves to turbulence attenuation of small heavy particles in a vertically orientated backward-facing step. The particles have material densities

much larger than the fluid ($\rho_p \gg \rho_f$) and diameters smaller than the Kolmogorov length scale over the moderately dilute range $\mathcal{O}(10^{-4})$.

The RA-TFM of Fox [21] is implemented in OpenFOAM and applied to the aforementioned flow configuration. The model predictions are compared against benchmark experimental data of Fessler and Eaton [18, 19]. In addition, predictions are also compared against the model of Peirano and Leckner [40] to highlight the importance of separating correlated and uncorrelated motion. Analysis is carried out on the mean particle stream-wise velocities and the fluctuation intensity of both the particle and fluid phases. Applying the RA-TFM to wall-bounded flow requires physical wall boundary conditions for the particle turbulent quantities, k_p, ε_p and $\langle\Theta\rangle_p$. To this end the Johnson and Jackson [31] boundary conditions were recently extended for the RA-TFM by Capecelatro et al. [8] and are implemented and applied here to describe the particle-wall interaction.

The paper is organised as follows; in the following section the numerical model is presented. This contains the RA-TFM in which the governing equations for each phase are presented along with the fully coupled turbulence models. Next, the wall boundary conditions used in this work are presented in their implemented form. Following this the numerical implementation of the RA-TFM into OpenFOAM is provided along with a description of the turbulence modelling implementation. Section 3 presents the results and discussion with the final section providing the conclusions.

2. Numerical Model

Here we begin by presenting the Reynolds-averaged transport equations from Fox [21]. The RA transport equations are presented in their conservative form with closures found in Table 5. For clarity the PA notation has been dropped and the PA variables along with their definitions can be found in Table 6. The particle phase continuity equation reads:

$$\frac{\partial \alpha_p \rho_p}{\partial t} + \nabla \cdot \alpha_p \rho_p \mathbf{u}_p = 0 \tag{1}$$

Where α_p is the volume fraction of particles, ρ_p is the density of the particles and $\mathbf{u}_p$ is the particle phase velocity.

The momentum balance equation for the RA particulate phase is given as:

$$\begin{aligned}\frac{\partial \alpha_p \rho_p \mathbf{u}_p}{\partial t} + \nabla \cdot \alpha_p \rho_p \mathbf{u}_p \mathbf{u}_p = \nabla \cdot 2(\mu_p + \mu_{pt})\overline{\mathbf{S}}_\mathbf{p} + \beta\Big[(\mathbf{u}_f - \mathbf{u}_p) - \frac{\nu_{ft}}{\mathrm{Sc}_{fs}\alpha_p\alpha_f}\nabla\alpha_p\Big] \\ -\nabla\Big(p_p + \frac{2}{3}\alpha_p\rho_p k_p\Big) - \alpha_p \nabla p_f + \alpha_p\rho_p\Big[1 - C_p\alpha_f\Big(1 - \frac{\rho_f}{\rho_p}\Big)\Big]\mathbf{g}\end{aligned} \tag{2}$$

Where the first term on the right hand side (RHS) contains the diffusive viscosity associated with the material viscosity and the particle turbulent viscosity. The forms for these are analogous to those of a fluid and can be found in Table 5. The second term is the momentum transfer term and contains both the slip velocity and a turbulent dispersion term. Through the denominator of the dispersion term $\mathrm{Sc}_{fp} = (k_f/k_p)^{1/2}$ a Stokes number (St) dependency is introduced which accounts for dispersion for moderate to large St. The form of this equation enforces the correct behaviour, when there is a small St the particle turbulent kinetic energy $k_p \to k_f$ thus returning 1; for a large St where k_p is small this represents a large value reducing the amount of dispersion i.e. the particles remain correlated with the fluid.

The third term is the pressure gradient along with the so-called turbulent pressure, with the fourth term being the covariance of the volume fraction and the fluid-pressure gradient. This term appears in both momentum equations and is typically assumed to be negligible. The last term contains the body forces (i.e. gravity) and the velocity-fluid-pressure-gradient covariance term. This term represents the correlations between the velocity and pressure gradients which arise from buoyancy.

The fluid phase continuity equation reads:

$$\frac{\partial \alpha_f \rho_f}{\partial t} + \nabla \cdot \alpha_f \rho_f \mathbf{u}_f = 0 \tag{3}$$

The momentum balance equation for the RA fluid phase is given as:

$$\frac{\partial \alpha_f \rho_f \mathbf{u}_f}{\partial t} + \nabla \cdot \alpha_f \rho_f \mathbf{u}_f \mathbf{u}_f = \nabla \cdot 2(\mu_f + \mu_{ft}) \overline{\mathbf{S}}_\mathbf{f} + \beta \Big[(\mathbf{u}_p - \mathbf{u}_f) + \frac{\nu_{ft}}{\mathrm{Sc}_{fs} \alpha_p \alpha_f} \nabla \alpha_p \Big] - \nabla \Big(\alpha_f p_f + \frac{2}{3} \alpha_f \rho_f k_f \Big) + \alpha_p \nabla p_f + \alpha_f \rho_f \Big[1 + C_p \alpha_p \Big(\frac{\rho_p}{\rho_f} - 1 \Big) \Big] \mathbf{g} \tag{4}$$

The momentum equations are symmetric with opposite pressure gradients, hence the corresponding term in the particle momentum equation (2) are defined in the same manner but with respect the fluid phase.

The RA turbulent kinetic energy transport equation for the fluid-phase takes the form:

$$\frac{\partial \alpha_f \rho_f k_f}{\partial t} + \nabla \cdot \alpha_f \rho_f k_f \mathbf{u}_f = \nabla \cdot \Big(\mu_t + \frac{\mu_{ft}}{\sigma_{fk}} \Big) \nabla k_f + \alpha_f \rho_f \Pi_f - \alpha_f \rho_f \varepsilon_f + 2\beta(k_{fp} - k_f) + \alpha_p \rho_p \Pi_{fp} + \alpha_p \rho_p \Pi_{\rho f} \tag{5}$$

The first term on the RHS is the fluid-phase turbulent kinetic energy flux. The second term Π_f represents kinetic energy production due to mean shear with the third term being the turbulent kinetic energy dissipation. The remaining three terms are the coupling terms: velocity correlations, mean slip and volume-fraction-velocity correlations, respectively.

The RA turbulent kinetic energy dissipation transport equation for the fluid-phase reads as:

$$\frac{\partial \alpha_f \rho_f \varepsilon_f}{\partial t} + \nabla \cdot \alpha_f \rho_f \varepsilon_f \mathbf{u}_f = \nabla \cdot \Big(\mu_t + \frac{\mu_{ft}}{\sigma_{fk}} \Big) \nabla \varepsilon_f + \frac{\varepsilon_f}{k_f} \Big[C_1 \alpha_f \Pi_f - C_2 \alpha_f \rho_f \varepsilon_f \Big] + 2C_3 \beta(\varepsilon_{fp} - \varepsilon_f) + C_4 \frac{\varepsilon_p}{k_p} \alpha_p \rho_p \Pi_{fp} + C_5 \frac{\varepsilon_p}{k_p} \alpha_p \rho_p \Pi_{\rho f} \tag{6}$$

The first term on the RHS is the fluid-phase turbulent kinetic dissipation energy flux. The second term Π_f is kinetic energy production due to mean shear with the third term is dissipation. The remaining three terms are the coupling terms: velocity correlations, mean slip and volume-fraction-velocity correlations, respectively. The forms of these are as follows:

$$\Pi_f = 2\nu_{ft} \overline{\mathbf{S}}_\mathbf{f} : \overline{\mathbf{S}}_\mathbf{f} + \frac{2}{3} k_f \nabla \cdot \mathbf{u}_f \tag{7}$$

$$\Pi_{fp} = \Big[C_g(\mathbf{u}_p - \mathbf{u}_f) - \frac{\nu_{ft}}{Sc_{fp} \alpha_p \alpha_f} \nabla \alpha_p \Big] \cdot \Big[\beta(\mathbf{u}_p - \mathbf{u}_f) + \frac{1}{\rho_p} \nabla p_f \Big] \tag{8}$$

$$\Pi_{\rho f} = C_\rho\Big(1 - \frac{\rho_f}{\rho_p}\Big)\Big[C_g\alpha_p\alpha_f(\mathbf{u}_p - \mathbf{u}_f) - \frac{\nu_{ft}}{Sc_{fp}}\nabla\alpha_p\Big]\cdot\mathbf{g} \tag{9}$$

Where Π_f is the production of the turbulent kinetic energy, Π_{fp} is due to mean slip and $\Pi_{\rho f}$ is due to volume-fraction-velocity correlations. The coupling terms take the form of $k_{fp} = \beta_k\sqrt{k_f k_p}$ and $\varepsilon_{fp} = \beta_\varepsilon\sqrt{\varepsilon_f\varepsilon_p}$. Where correlation coefficients are $0 < \beta_k,\ \beta_\varepsilon \leq 1$. These terms represent the fluid-velocity covariance and their exact closure is still uncertain, a detailed discussion on this point can be found in [21]. This form is adopted as it shows correct limiting behaviour for large St as well as diminishing correctly in the absence of the particulate phase.

The RA particle-phase turbulent kinetic energy reads as:

$$\begin{aligned}\frac{\partial\alpha_p\rho_p k_p}{\partial t} + \nabla\cdot\alpha_p\rho_p k_p\mathbf{u}_p = \nabla\cdot\Big(\mu_p + \frac{\mu_{pt}}{\sigma_{pk}}\Big)\nabla k_p + \alpha_p\rho_p\Pi_p - \alpha_p\rho_p\varepsilon_p \\ +2\beta(k_{fp} - k_p) + \alpha_p\rho_p\Pi_{\rho p}\end{aligned} \tag{10}$$

The first term on the RHS is the particle-phase turbulent kinetic energy flux. The second term Π_p is kinetic energy production due to mean shear with the third term being the particle turbulent kinetic energy dissipation. The remaining two terms are the coupling terms: velocity correlations, and the combination of the buoyancy induced and mean slip terms.

The RA particle-phase turbulent kinetic energy dissipation transport equation reads:

$$\begin{aligned}\frac{\partial\alpha_p\rho_p\varepsilon_p}{\partial t} + \nabla\cdot\alpha_p\rho_p\varepsilon_p\mathbf{u}_p = \nabla\cdot\Big(\mu_p + \frac{\mu_{pt}}{\sigma_{pk}}\Big)\nabla\varepsilon_p + \frac{\varepsilon_p}{k_p}(C_1\alpha_p\rho_p\Pi_p - C_2\alpha_p\rho_p\varepsilon_p) \\ +2C_3\beta(\varepsilon_{fp} - \varepsilon_p) + C_5\frac{\varepsilon_p}{k_p}\alpha_p\rho_p\Pi_{\rho p}\end{aligned} \tag{11}$$

The first term on the RHS is the particle phase turbulent kinetic dissipation energy flux. The second term Π_p is kinetic energy production due to mean shear with the third term being its dissipation. The remaining two terms are the coupling terms: velocity correlations, and the combination of the buoyancy induced and mean slip terms. The second term contains, Π_p which is the production of the turbulent kinetic energy and is expressed as:

$$\Pi_p = 2\nu_{pt}\overline{\mathbf{S}}_\mathbf{p} : \overline{\mathbf{S}}_\mathbf{p} + \frac{2}{3}k_p\nabla\cdot\mathbf{u}_p \tag{12}$$

It should be noted here that the final term on the RHS is a compressive term that appears in compressible turbulence modelling and plays a similar role of the bulk viscosity found in the typical granular temperature formulations in the literature [40],

[51]. Finally, the buoyancy-induced source term $\Pi_{\rho f}$ is added to the mean slip Π_{fp} to be reformulated as $\Pi_{\rho p}$ which is read as:

$$\Pi_{\rho p} = C_\rho C_p \alpha_f \Big(1 - \frac{\rho_f}{\rho_p}\Big)(\mathbf{u}_p - \mathbf{u}_f) \cdot \mathbf{g} \tag{13}$$

The granular temperature equation reads as:

$$\begin{aligned} \frac{3}{2}\Big[\frac{\partial \alpha_p \rho_p \Theta_p}{\partial t} + \nabla \cdot \alpha_p \rho_p \Theta_p \mathbf{u}_p\Big] = \nabla \cdot \Big(\kappa_\Theta + \frac{3\mu_{pt}}{2Pr_{pt}}\Big)\nabla \Theta_p + 2\mu_p \overline{\mathbf{S}}_\mathbf{p} : \overline{\mathbf{S}}_\mathbf{p} \\ -p_p \nabla \cdot \mathbf{u}_p + \alpha_p \rho_p \varepsilon_p - 3\beta \Theta_p - \gamma \end{aligned} \tag{14}$$

The first term on the RHS is the PA granular temperature flux which is made up of two contributions, the granular temperature flux and the turbulent granular flux. The former is the granular conductivity of which there are various formulations in the literature. Here the formulation of Syamlal and O'Brien [48] is used as it correctly tends to zero in the dilute limit [51]. The latter term is the turbulent flux and includes the particle turbulent viscosity. The second term is a laminar source term due to viscous stresses. The third term is a pressure dilation term which accounts for compressibility. The fourth term is of particular interest as it represents the turbulent particle kinetic energy dissipation which appears here as a positive source term. The physical interpretation of this means that as large scale particle turbulent kinetic energy is dissipated, small scale granular temperature is produced. The two remaining terms represent decrease of granular temperature due to drag and decrease of granular temperature due to inelastic collisions.

Table 1: Turbulence model parameters.

C_p	C_g	C_ρ	C_1	C_2	C_3	C_4	C_5	β_k	β_ε	$C_{f\mu}$	$C_{p\mu}$
1	0	1	1.44	1.92	1	1	1	1	1	0.09	0.09

The full form of the equations have been presented here with no mention of their relevance to the flow regime being simulated in this work. As the density ratio is high the buoyancy induced terms are negligible. The coefficient $C_g \to 0$ due to the small mass loading used in this work, a more thorough discussion on this topic can be found in [6, 7, 21]. The buoyancy terms were indeed found to be negligible but are retained here to show their solution treatment. Similarly, the compressible turbulence correction terms depend on the particle-phase Mach number, which is expected to be large for large St. Given the St values used in this study this is not

expected to be the case but have been retained. A thorough discussion on this topic is provided in Section 3.4.1.

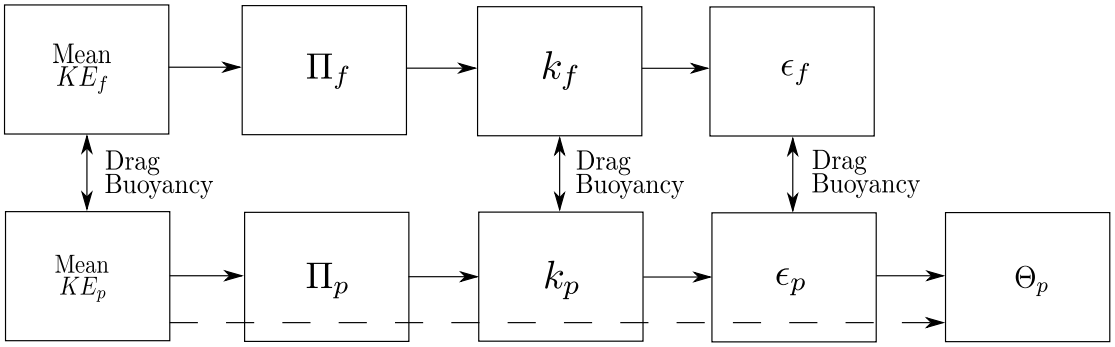

Figure 1: Schematic showing the energy cascade between each variable within the multiphase model [21]. The interaction between each quantity is shown along with their respective energy transfer mechanisms. The dashed line represents the energy flow in the (mesoscale) laminar model.

Fig. 1 shows an overall picture of the RA-TFM. As can be seen the energy cascade is almost identical in both phases. Starting with the mean particle kinetic energy $\frac{1}{2}\mathbf{u}_p \cdot \mathbf{u}_p$, the energy transfer to the turbulent particle kinetic energy is given by the production term which is Π_p i.e. the shear. This then generates k_p and is dissipated by the turbulent kinetic energy dissipation equation. Finally, this dissipation term ε_p appears in the granular temperature Θ_p as a positive source term, meaning that as the particle turbulent kinetic energy dissipates, granular energy is produced. As can be seen both turbulent quantities interact via drag and buoyancy terms in the same way the governing equations do. If there is dissipation due to collisions then the granular temperature is reduced due to particle heating.

2.1. Particle wall boundary conditions

The wall boundary conditions for the particle phase require additional modelling. Recently, Capecelatro et al. [8] started from the Johnson and Jackson [31] wall boundary conditions and derived wall boundary conditions for the particle turbulence quantities k_p, ε_p and Θ_p. Here we present the boundary conditions in their implemented form applicable for Finite-Volume-Method codes and begin with the wall boundary condition for the particle velocity $\mathbf{u}_p$.

$$\mathbf{n} \cdot \overline{\boldsymbol{\sigma}}_p \nabla \mathbf{u}_{p,w} = -\frac{\pi}{6} \frac{\alpha_p}{\alpha_{p,max}} \phi \rho_p g_0 \sqrt{3\Theta_p} \mathbf{u}_{p,w} \tag{15}$$

Here we define $\mathbf{u}_{p,w}$ as the particle slip velocity parallel to the wall, $\mathbf{u}_{p,w} = \mathbf{u}_p - \mathbf{u}_w$ with $\mathbf{u}_w$ defined as the wall velocity. Where $\overline{\boldsymbol{\sigma}}_p$ is the particle viscous stress tensor and we denote $\mathbf{n}$ as the unit vector normal to the wall. Then equation 15 is recast into a more compact form

$$\mathbf{n} \cdot \overline{\boldsymbol{\sigma}}_p \nabla \mathbf{u}_{p,w} = -\mathcal{D}_w \mathbf{u}_{p,w} \tag{16}$$

where the term $\mathcal{D}_w = \phi \mathcal{V}_w$ representing ϕ, the specularity coefficient and the term $\mathcal{V}_w = \frac{\pi}{6} \frac{\alpha_p}{\alpha_{p,max}} \rho_p \sqrt{3\Theta_p} g_0$ which contains the tangential momentum $\frac{\pi}{6} \frac{\alpha_p}{\alpha_{p,max}} \rho_p$ (omitting the particle slip velocity parallel to the wall $\mathbf{u}_{p,w}$) and the collisional frequency $\sqrt{3\Theta_p} g_0$. This boundary condition prescribes a particle partial-slip velocity at the wall. From this condition it follows that the components of the Reynolds stress tensor $\langle \mathbf{u}_p'' \mathbf{u}_p'' \rangle_p$ need not be zero at the wall unlike in the fluid phase. As we are interested in modelling the particle-wall interaction of the particle turbulent kinetic energy k_p we assume isotropy in the fluctuating components.

$$k_p = \frac{1}{2} (\mathbf{u}_{p,x}''^2 + \mathbf{u}_{p,y}''^2 + \mathbf{u}_{p,z}''^2) \tag{17}$$

Equating the principal Reynolds stress components ($\mathbf{u}_{p,x}''^2 \equiv \mathbf{u}_{p,y}''^2 \equiv \mathbf{u}_{p,z}''^2$) one arrives at $k_p = 1.5\, \mathbf{u}_p''^2$ and substituting into Equation 16 by employing the PA decomposition (see Table 6) the wall boundary condition for k_p reads

$$\mathbf{n} \cdot \overline{\boldsymbol{\sigma}}_p \nabla k_p = -2\mathcal{D}_w k_p \tag{18}$$

Following on from this a condition for the particle turbulent kinetic energy dissipation rate ε_p can be prescribed:

$$\mathbf{n} \cdot \overline{\boldsymbol{\sigma}}_p \nabla \varepsilon_p = -2\mathcal{D}_w \varepsilon_p \tag{19}$$

Finally, the wall boundary condition for the granular temperature can be found by Reynolds averaging the Johnson and Jackson [31] which reads as

$$\mathbf{n} \cdot \boldsymbol{q}_\Theta \frac{3}{2} = \phi \mathcal{D}_w |\mathbf{u}_{p,w}|^2 - \frac{3}{2} \mathcal{D}_\kappa \Theta_p \tag{20}$$

where $\boldsymbol{q}_\Theta$ is the granular temperature flux and with $\mathcal{D}_\kappa = (1 - \mathrm{e}_w)^2 \mathcal{D}_w$ and e_w is the restitution of coefficient with the wall. It follows from this that this term represents the energy loss through particle collisions with the wall. The first term on the RHS represents the increase of the granular temperature due to the relative velocity with the wall. This means that the slip condition at the wall is capable of increasing the granular temperature. The particle-wall coefficient, e_w was set equal to 0.9. The specularity coefficient used throughout was, $\phi = 0.001$ and the influence of this parameter is discussed in Section 3.3.4.

2.2. Numerical implementation

Here we follow the phase intensive formulation of Rusche [43], Weller [55]. We rewrite the equations in their non-conservative form by expanding both the convective term and dividing by density and volume fraction.

Additionally, the phase respective Reynolds stress tensor is formulated by grouping the kinematic and turbulent viscosity into an effective viscosity, $\nu_{\text{eff,i}} = \nu_i + \nu_{it}$ and employing the Boussinesq hypothesis. Now, we can write the Reynolds stress tensor in the form:

$$\overline{\mathbf{R}}_{\text{eff,p}} = -2\nu_{\text{eff,p}}\overline{\mathbf{S}}_{\mathbf{p}} + \frac{2}{3}\nu_{\text{eff,p}}\mathbf{I}\nabla\cdot\mathbf{u}_p + \frac{2}{3}\mathbf{I}k_p \tag{21}$$

$$\overline{\mathbf{R}}_{\text{eff,f}} = -2\nu_{\text{eff,f}}\overline{\mathbf{S}}_{\mathbf{f}} + \frac{2}{3}\nu_{\text{eff,f}}\mathbf{I}\nabla\cdot\mathbf{u}_f + \frac{2}{3}\mathbf{I}k_f \tag{22}$$

For simplicity the turbulent dispersion term is now denoted as $\mathscr{D}$, separating the drag contributions into explicit and implicit terms and dividing by both the phase fraction and density we are left with:

$$\begin{aligned}\frac{\partial\mathbf{u}_p}{\partial t} + \nabla\cdot(\mathbf{u}_p\mathbf{u}_p) - \mathbf{u}_p\nabla\cdot\mathbf{u}_p + \frac{\nabla\alpha_p}{\alpha_p+\delta}\cdot\overline{\mathbf{R}}^c_{\text{eff,p}} + \nabla\cdot\overline{\mathbf{R}}^c_{\text{eff,p}} - \nabla\cdot(\nu_{\text{eff,p}}\nabla\mathbf{u}_p) + \frac{\beta\mathbf{u}_p}{\alpha_p\rho_p} \\ -\nabla\cdot\Big(\nu_{\text{eff,p}}\frac{\nabla\alpha_p}{\alpha_p+\delta}\mathbf{u}_p\Big) + \mathbf{u}_p\nabla\cdot\Big(\nu_{\text{eff,p}}\frac{\nabla\alpha_p}{\alpha_p+\delta}\Big) \\ = \frac{\beta\mathbf{u}_f}{\alpha_p\rho_p} - \frac{\beta\mathscr{D}\nabla\alpha_p}{\alpha_p\rho_p} - \frac{\nabla p_p}{\alpha_p\rho_p} - \frac{\nabla p_f}{\rho_p} + \mathbf{g} - \alpha_f\Big(1-\frac{\rho_f}{\rho_p}\Big)\mathbf{g}\end{aligned} \tag{23}$$

$$\begin{aligned}\frac{\partial\mathbf{u}_f}{\partial t} + \nabla\cdot(\mathbf{u}_f\mathbf{u}_f) - \mathbf{u}_f\nabla\cdot\mathbf{u}_f + \frac{\nabla\alpha_f}{\alpha_f+\delta}\cdot\overline{\mathbf{R}}^c_{\text{eff,f}} + \nabla\cdot\overline{\mathbf{R}}^c_{\text{eff,f}} - \nabla\cdot(\nu_{\text{eff,f}}\nabla\mathbf{u}_f) + \frac{\beta\mathbf{u}_f}{\alpha_f\rho_f} \\ -\nabla\cdot\Big(\nu_{\text{eff,f}}\frac{\nabla\alpha_f}{\alpha_f+\delta}\mathbf{u}_f\Big) + \mathbf{u}_p\nabla\cdot\Big(\nu_{\text{eff,f}}\frac{\nabla\alpha_f}{\alpha_f+\delta}\Big) \\ = \frac{\beta\mathbf{u}_p}{\alpha_f\rho_f} + \frac{\beta\mathscr{D}\nabla\alpha_p}{\alpha_f\rho_f} - \frac{\nabla p_f}{\rho_f} - \frac{\alpha_p\nabla p_f}{\alpha_f\rho_f} + \mathbf{g} + \alpha_p\Big(\frac{\rho_p}{\rho_f}-1\Big)\mathbf{g}\end{aligned} \tag{24}$$

where δ is introduced to avoid a division by zero. As it can be seen from the system of equations in Eqs. 2 & 4 no diffusive flux exists that can be treated implicitly. This can have advantages when solving the equations i.e enhanced matrix positively and diagonal dominance. Therefore, following Weller [55], Rusche [43] the Reynolds stress term can be rewritten into a diffusive and corrective component:

$$
\begin{aligned}
\overline{\mathbf{R}}_{\text{eff,i}} &= \overline{\mathbf{R}}_{\text{eff,i}} + \nu_{\text{eff,i}}\nabla\mathbf{u}_i - \nu_{\text{eff,i}}\nabla\mathbf{u}_i \\
&= -\nu_{\text{eff,i}}(\nabla\mathbf{u}_i + \nabla^T\mathbf{u}_i) + \frac{2}{3}\nu_{\text{eff,i}}\mathbf{I}\nabla\cdot\mathbf{u}_i \\
&+ \frac{2}{3}\mathbf{I}k_i + \nu_{\text{eff,i}}\nabla\mathbf{u}_i - \nu_{\text{eff,i}}\nabla\mathbf{u}_i \\
&= (-\nu_{\text{eff,i}}\nabla^T\mathbf{u}_i + \frac{2}{3}\nu_{\text{eff,i}}\mathbf{I}\nabla\cdot\mathbf{u}_i + \frac{2}{3}k_i\mathbf{I}) - \nu_{\text{eff,i}}\nabla\mathbf{u}_i \\
&= \overline{\mathbf{R}}^c_{\text{eff,i}} - \nu_{\text{eff,i}}\nabla\mathbf{u}_i
\end{aligned}
\tag{25}
$$

It is important to clarify the behaviour of terms with the volume fraction in their denominator. For the first contribution due to drag i.e. the third term on the RHS the coefficient β contains $\alpha_p\alpha_f$ which ensures the correct behavior of the function as $\alpha_p \to 0$. The second term containing turbulent dispersion contains the gradient of volume fraction which in the limit $\alpha_p \to 0$ means that the ratio approaches zero. Finally, the fluid velocity-pressure-covariance term contains the volume fraction in its denominator, however due to the particle packing limit ensured by the particle's structural properties the volume fraction of the fluid phase does not approach 0.

2.3. Discretisation of the intensive momentum equations

First, we discretise the left hand side of the equation which contains the convective and diffusive transport terms.

$$
\begin{aligned}
\mathcal{T}_p := \Big[\frac{\partial\mathbf{u}_p}{\partial t}\Big] + \Big[\nabla\cdot(\mathbf{u}_p[\mathbf{u}_p])\Big] - \Big[(\nabla\cdot\mathbf{u}_p)[\mathbf{u}_p]\Big] + \frac{\nabla\alpha_p}{\alpha_p+\delta}\cdot\overline{\mathbf{R}}^c_{\text{eff,p}} + \nabla\cdot\overline{\mathbf{R}}^c_{\text{eff,p}} \\
-\Big[\nabla\cdot(\nu_{\text{eff,p}}\nabla[\mathbf{u}_p])\Big] - \Big[\nabla\cdot(\nu_{\text{eff,p}}\frac{\nabla\alpha_p}{\alpha_p+\delta}[\mathbf{u}_p])\Big] \\
-\Big[\nabla\cdot(\nu_{\text{eff,p}}\frac{\nabla\alpha_p}{\alpha_p+\delta})[\mathbf{u}_p])\Big] + \Big[\frac{\beta\mathbf{u}_p}{\alpha_p\rho_p}\Big]
\end{aligned}
\tag{26}
$$

$$
\begin{aligned}
\mathcal{T}_f := \Big[\frac{\partial\mathbf{u}_f}{\partial t}\Big] + \Big[\nabla\cdot(\mathbf{u}_f[\mathbf{u}_f])\Big] - \Big[(\nabla\cdot\mathbf{u}_f)[\mathbf{u}_f]\Big] + \frac{\nabla\alpha_f}{\alpha_f+\delta}\cdot\overline{\mathbf{R}}^c_{\text{eff,f}} + \nabla\cdot\overline{\mathbf{R}}^c_{\text{eff,f}} \\
-\Big[\nabla\cdot(\nu_{\text{eff,f}}\nabla[\mathbf{u}_f])\Big] - \Big[\nabla\cdot(\nu_{\text{eff,f}}\frac{\nabla\alpha_f}{\alpha_f+\delta}[\mathbf{u}_f])\Big] \\
-\Big[\nabla\cdot(\nu_{\text{eff,f}}\frac{\nabla\alpha_f}{\alpha_f+\delta})[\mathbf{u}_f])\Big] + \Big[\frac{\beta\mathbf{u}_f}{\alpha_f\rho_f}\Big]
\end{aligned}
\tag{27}
$$

where $[\cdot]$ is the implicit dicretisation of the term, $\mathcal{T}_p$ & $\mathcal{T}_f$ represents the numerical coefficients of each respective algebraic system given by the discretisation. The

second and third terms on the RHS represent convection and have been split up into a convection term minus a divergence terms as it enhances boundedness of the solution.

$\mathcal{T}_p$ & $\mathcal{T}_f$ represents the system of algebraic equations from the discretisated Eqs. 26 & 27 which appear in the form,

$$(\mathcal{T}_p)_{coeffs}\mathbf{u}_p = (\mathcal{T}_p)_s \tag{28a}$$
$$(\mathcal{T}_f)_{coeffs}\mathbf{u}_f = (\mathcal{T}_f)_s \tag{28b}$$

This discretised form of the momentum equations will be revisited once the source terms on the RHS are addressed.

Now addressing the RHS of Eq. 23 & 24 which reads as

$$... = \frac{\beta\mathbf{u}_f}{\alpha_p\rho_p} - \frac{\beta\mathscr{D}\nabla\alpha_p}{\alpha_p\rho_p} - \frac{\nabla p_p}{\alpha_p\rho_p} - \frac{\nabla p_f}{\rho_p} + \mathbf{g} - \alpha_f\Big(1 - \frac{\rho_f}{\rho_p}\Big)\mathbf{g} \tag{29a}$$
$$... = \frac{\beta\mathbf{u}_p}{\alpha_f\rho_f} + \frac{\beta\mathscr{D}\nabla\alpha_p}{\alpha_f\rho_f} - \frac{\nabla p_f}{\rho_f} - \frac{\alpha_p\nabla p_f}{\alpha_f\rho_f} + \mathbf{g} + \alpha_p\Big(\frac{\rho_p}{\rho_f} - 1\Big)\mathbf{g} \tag{29b}$$

denoting the buoyancy terms to be $\mathbf{g}_p^* = \mathbf{g}(1 - \alpha_p(1 - \frac{\rho_f}{\rho_p}))$ & $\mathbf{g}_f^* = \mathbf{g}(1 + \alpha_p(\frac{\rho_p}{\rho_f} - 1)$ we can write

$$... = \frac{\beta\mathbf{u}_f}{\alpha_p\rho_p} - \frac{\beta\mathscr{D}\nabla\alpha_p}{\alpha_p\rho_p} - \frac{\nabla p_f}{\rho_p} - \frac{\nabla p_p}{\alpha_p\rho_p} + \mathbf{g}_p^* \tag{30a}$$
$$... = \frac{\beta\mathbf{u}_p}{\alpha_f\rho_f} + \frac{\beta\mathscr{D}\nabla\alpha_p}{\alpha_f\rho_f} - \frac{\nabla p_f}{\rho_f} - \frac{\alpha_p\nabla p_f}{\alpha_f\rho_f} + \mathbf{g}_f^* \tag{30b}$$

Following the solution procedure of Weller [55] all terms on the RHS are evaluated at cell faces. In order to avoid checker-boarding in the solution, which is a prevalent problem on collocated grids due to the storage of values at cell centres and interpolating onto the face, the group of terms on the RHS are treated in a Rhie-Chow like manner Rhie and Chow [42].

2.4. Phase momentum flux correction equations

Now a semi-discretised formulation of both the particle- and fluid-phase can be written. Invoking Eqs. 28 and splitting up the total coefficients appearing in each system into diagonal and explicit $\mathbf{H}$ [30] coefficients. The latter consisting of two parts, the neighbouring coefficients (multiplied by its respective phase velocity) and the source terms, $\mathbf{H}_i = -(\mathbf{A}_i)_N\mathbf{u}_i + (\mathbf{A}_i)_S$. The equations can then be written as:

$$\mathbf{A}_p\mathbf{u}_p = \mathbf{H}_p + \frac{\beta\mathbf{u}_f}{\alpha_p\rho_p} - \frac{\beta\mathscr{D}\nabla\alpha_p}{\alpha_p\rho_p} - \frac{\nabla p_f}{\rho_p} - \phi_{p,p} + \mathbf{g}_p^* \tag{31a}$$

$$\mathbf{A}_f\mathbf{u}_f = \mathbf{H}_f + \frac{\beta\mathbf{u}_p}{\alpha_f\rho_f} + \frac{\beta\mathscr{D}\nabla\alpha_p}{\alpha_f\rho_f} - \frac{\nabla p_f}{\rho_f} - \phi_{f,g} + \mathbf{g}_f^* \tag{31b}$$

Rearranging Eqs. 31 gives the phase momentum correction equations, note these equations are not used in the solution algorithm, but are required to derive a flux predictor and corrector:

$$\mathbf{u}_p = \frac{\mathbf{H}_p}{\mathbf{A}_p} + \frac{\beta\mathbf{u}_f}{\alpha_p\rho_p\mathbf{A}_p} - \frac{\beta\mathscr{D}\nabla\alpha_p}{\alpha_p\rho_p\mathbf{A}_p} - \frac{\nabla p_f}{\rho_p\mathbf{A}_p} - \frac{\phi_{p,p}}{\mathbf{A}_p} + \frac{\mathbf{g}_p^*}{\mathbf{A}_p} \tag{32a}$$

$$\mathbf{u}_f = \frac{\mathbf{H}_f}{\mathbf{A}_f} + \frac{\beta\mathbf{u}_p}{\alpha_f\rho_f\mathbf{A}_f} + \frac{\beta\mathscr{D}\nabla\alpha_p}{\alpha_f\rho_f\mathbf{A}_f} - \frac{\nabla p_f}{\rho_f\mathbf{A}_f} - \frac{\phi_{f,g}}{\mathbf{A}_f} + \frac{\mathbf{g}_f^*}{\mathbf{A}_f} \tag{32b}$$

2.5. Construction of the pressure equation

In order to derive a pressure equation the continuity equation is enforced globally. The global continuity equation thus reads:

$$\nabla \cdot [(\alpha_p)_f\phi_p + (\alpha_f)_f\phi_f] = 0 \tag{33}$$

where the subscript $()_f$ denotes the face value and $\phi_i = (\mathbf{u}_i)_f \cdot \mathbf{S}_f$ is the volumetric face flux i.e. the sum of all the fluxes over a control volume. From here the phase fluxes for each phase are found by interpolating the momentum correction equation (Eqs. 32) onto face centres. Using central differencing, we can write

$$\phi_p = \phi_p^* - \left(\frac{1}{\rho_p\mathbf{A}_p}\right)_f \nabla_f^\perp p_f \cdot \mathbf{S}_f \tag{34a}$$

$$\phi_f = \phi_f^* - \left(\frac{1}{\rho_f\mathbf{A}_f}\right)_f \nabla_f^\perp p_f \cdot \mathbf{S}_f \tag{34b}$$

where the flux predictions ϕ_p^* & ϕ_f^* are given by

$$\begin{aligned}\phi_p^* = \left(\frac{\mathbf{H}_p}{\mathbf{A}_p}\right)_f \cdot \mathbf{S}_f + \left(\frac{\beta}{\alpha_p\rho_p\mathbf{A}_p}\right)_f \phi_f - \left(\frac{\beta\mathscr{D}}{\alpha_p\rho_p\mathbf{A}_p}\right)_f \nabla_f^\perp\alpha_p \cdot \mathbf{S}_f \\ - \left(\frac{1}{\mathbf{A}_p}\right)_f \nabla_f^\perp p_p \cdot \mathbf{S}_f + \left(\frac{1}{\mathbf{A}_p}\right)_f \mathbf{g}_p^* \cdot \mathbf{S}_f\end{aligned} \tag{35}$$

$$\phi_f^* = \left(\frac{\mathbf{H}_f}{\mathbf{A}_f}\right)_f \cdot \mathbf{S}_f + \left(\frac{\beta}{\alpha_f \rho_f \mathbf{A}_f}\right)_f \phi_p - \left(\frac{\beta \mathscr{D}}{\alpha_f \rho_f \mathbf{A}_f}\right)_f \nabla_f^{\perp} \alpha_p \cdot \mathbf{S}_f - \left(\frac{\alpha_p}{\alpha_f \rho_f \mathbf{A}_f}\right)_f \nabla_f^{\perp} p_f \cdot \mathbf{S}_f + \left(\frac{1}{\mathbf{A}_f}\right)_f \mathbf{g}_f^* \cdot \mathbf{S}_f \tag{36}$$

Now the pressure equation can be constructed by substituting Eq. 34 into Eq. 33 which reads:

$$\left[\nabla \cdot \left(D_p \nabla_f^{\perp}[p_f] \cdot \mathbf{S}_f\right)\right] = \nabla \cdot \left((\alpha_p)_f \phi_p^* + (\alpha_f)_f \phi_f^*)\right) \tag{37}$$

where

$$D_p = \left(\frac{\alpha_p}{\rho_p \mathbf{A}_p} + \frac{\alpha_f}{\rho_f \mathbf{A}_f}\right)_f, \tag{38}$$

and the pressure gradient has been discretised implicitly on the LHS as a diffusion term i.e. Laplacian. Essentially a shared or mixture pressure field is solved for, this ensures that continuity is obeyed throughout as the coupling is provided through the pressure equation. Once this equation has been solved the phase fluxes need to be updated to satisfy continuity, as in the predictor step the influence of the pressure gradient is removed, this can be achieved by invoking Eq. 34. From this stage the solution does not completely satisfy continuity as the velocities, which are stored at the cell centres, need to be updated with the influence of the pressure gradient.

This is achieved by invoking:

$$\mathbf{u}_p = \frac{\mathbf{H}_p}{\mathbf{A}_p} + \left[\phi_p^* - \left(\frac{1}{\rho_p \mathbf{A}_p}\right)_f \nabla_f^{\perp} p_f \cdot \mathbf{S}_f\right]_{f \to c} \tag{39a}$$

$$\mathbf{u}_f = \frac{\mathbf{H}_f}{\mathbf{A}_f} + \left[\phi_f^* - \left(\frac{1}{\rho_f \mathbf{A}_f}\right)_f \nabla_f^{\perp} p_f \cdot \mathbf{S}_f\right]_{f \to c} \tag{39b}$$

where the subscript $f \to c$ denotes a vector field reconstruction from face flux values to cell centre values. The influence of the gradient of pressure is incorporated into the reconstruction of the phase velocity - this ensures the phase velocity obeys continuity. Once this is completed the PISO loop is complete.

2.6. Solution of the phase-mixed continuity equation

In practice the phase-mixed continuity equation is solved first based on the initial conditions but for the sake of logical progression is presented now. Following Weller

[55] the particle phase continuity equation **??** can be reformulated as:

$$\frac{\partial \alpha_p}{\partial t} + \nabla \cdot (\mathbf{u}_T \alpha_p) + \nabla \cdot (\mathbf{u}_r \alpha_p \alpha_f) = 0 \tag{40}$$

where $\mathbf{u}_T = \alpha_p \mathbf{u}_p + \alpha_f \mathbf{u}_f$ is the mixture velocity and $\mathbf{u}_r = \mathbf{u}_p - \mathbf{u}_f$ is the relative velocity. This equation can then be discretised as

$$\left[\frac{\partial [\alpha_p]}{\partial t}\right] + \left[\nabla \cdot \left(\phi [\alpha_p]_f\right)\right] + \left[\nabla \cdot \left(\phi_{r,p} [\alpha_p]_f\right)\right] = 0 \tag{41}$$

where $\phi_{r,p} = (\alpha_f)_f \phi_r$ and $\phi_r = \phi_p - \phi_f$.

The second term on the LHS is ensured to be bounded between 0 and 1 due to the mixture flux, $\phi = (\mathbf{u}_p)_f \cdot \mathbf{S}_f + (\mathbf{u}_f)_f \cdot \mathbf{S}_f$ satisfying the mixture continuity equation. The third term is bounded by employing ϕ_r in the convective scheme by interpolating α_p to the face and $-\phi_r$ in the face interpolation of α_f. This system is solved using the the Multi-dimensional Universal Limiter with Explicit Solution (MULES) [59] which is a flux-corrected transport algorithm which enhances robustness, stability and convergence.

The numerical procedure adopted in the segregated algorithm:

1. Solve the volume fraction (Eq. 41).
2. Construct $\mathbf{A}_i$ in each phase (Eqs. 28).
3. Enter PISO-Loop:
   (a) Predict fluxes using Eqs. 35 & 36.
   (b) Construct and solve the pressure equation (Eq. 37).
   (c) Correct the phase fluxes using Eqs. 34.
   (d) Reconstruct the phase velocities using Eqs. 39.
4. Solve the system of phase energy equations

The $k_p - \varepsilon_p$ transport equation is implemented in a similar manner to the $k_f - \varepsilon_f$ transport equation. A thorough discussion of its implementation in OpenFOAM can be found in [37, 30, 43]. The coupling terms found in each equation are handled in a segregated manner due to the velocity-pressure solution treatment. From the solution of the aforementioned transport equations the granular temperature is then solved as the particle turbulence dissipation ε_p appears as a source term in the transport equation of granular temperature Θ_p.

2.7. Numerical solution

The open-source toolbox OpenFOAM [56] is used to solve the RA-TFM equations. To handle the pressure-velocity coupling the Pressure Implicit with Splitting Operators (PISO) algorithm [17, 29] is used. The volume fraction is solved using a Multi-dimensional Universal Limiter with Explicit Solution (MULES) [59] which is a flux-corrected transport algorithm which ensures robustness, stability and convergence.

2.8. Simulation cases

The computational domain is a two-dimensional channel section as seen in Fig. 2 which starts at 60h upstream of the step to allow the flow to fully develop and extends 30H downstream. The material constants for each respective case can be found in Table 2. As reported in the experiments the centreline velocity, U_0 is 10.5 ms^{-1} at the step (x/H =0) and this corresponded to an inlet value of 9.3 ms^{-1}. Mass loading is given by a uniform particle volume fraction across the inlet, this is achieved by assuming a constant particle-to-fluid velocity ratio. Wall functions for the fluid phase are used throughout and the effect of the particles on the boundary layer is not considered here. For the particle phase the boundary conditions described in Section 2.1 are used for the turbulent quantities. At the inlet a first estimate of the two turbulent quantities is determined as follows; $k_p = 1/3k_f$ and $\varepsilon_p = 1/3\varepsilon_f$ (for a more elaborate approach see [21]). For the granular temperature a small value is specified; $\Theta_p = 1.0\mathrm{x}10^{-8}\mathrm{m}^2\mathrm{s}^{-2}$ [51]. Calculations are carried out on a fully structured hexahedral mesh consisting of 11,253 cells with $\mathrm{y}^+ > 30$ along both walls. Refinement was introduced around the step resulting in the mesh cells sizes of 0.5 mm in the x and y direction, respectively.

Table 2: Table of simulated cases.

Case	Material	d_p [μm]	ρ_p [kg m^{-3}]	Mass loading	St	Re_p
1	glass	150	2500	20% and 40%	7.9	10.1
2	glass	90	2500	20%	3.8	2.9
3	copper	70	8800	10% and 40%	7.4	4.4

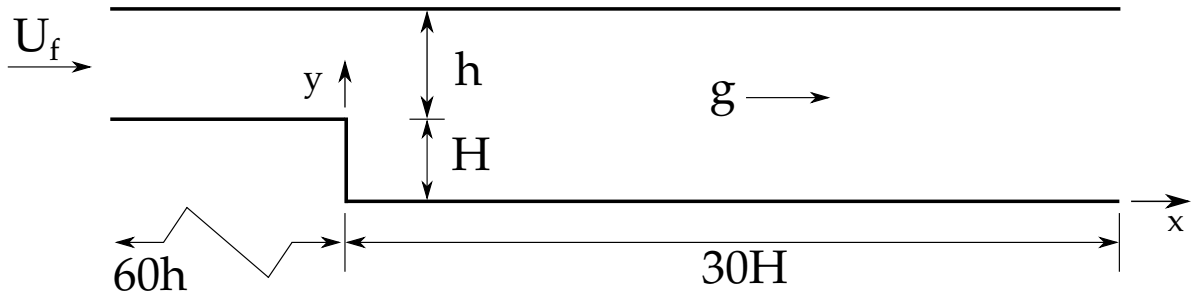

Figure 2: Schematic detailing the geometry used throughout, with h = 0.02m and H = 0.0267m.

3. Results and Discussion

The simulated results from the RA-TFM and the modified Peirano model (MPM) are compared against two sets of experimental data given by Fessler and Eaton [19] & Fessler and Eaton [18]. The MPM equations can be found in the Appendix. Mean quantities of particle velocity, fluid turbulence intensity and particle turbulence intensity are presented across three cases focusing on three particle classes (see Table 1). The measured velocity profiles start at the recirculation region (x/H = 2), continue through to the reattachment zone (x/H = 5), and finally the redevelopment region (x/H = 14) with measurements being taken in between.

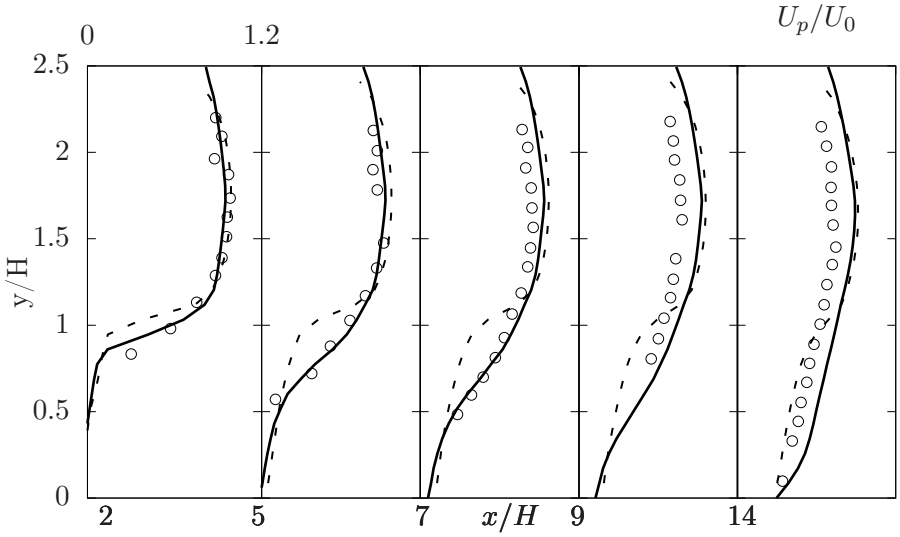

Figure 3: Stream-wise particle mean velocity for case 1. Solid line showing the RA-TFM and the dashed line showing the MPM. Data from Fessler and Eaton [18] with a mass-loading of 40%.

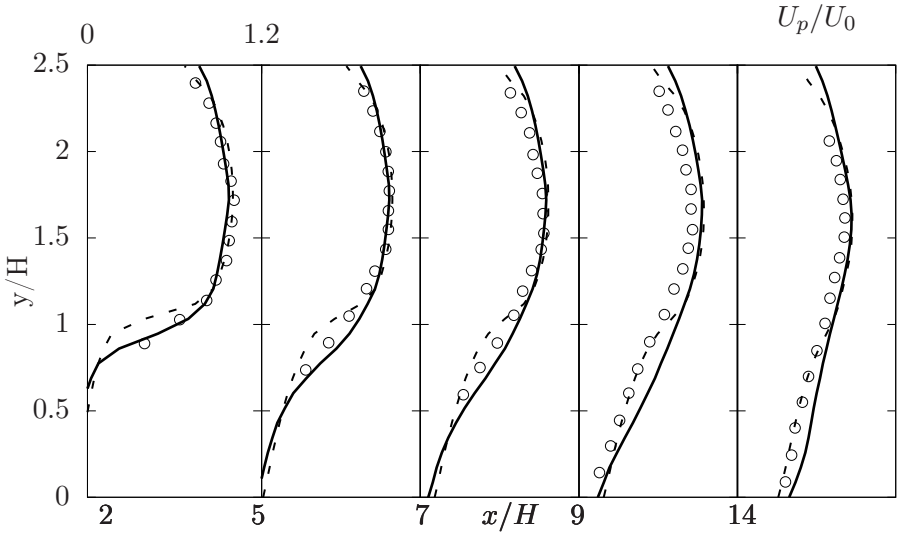

Figure 4: Stream-wise particle mean velocity for case 2. Solid line showing the RA-TFM and the dashed line showing the MPM. Data from Fessler and Eaton [18] with a mass-loading of 20%.

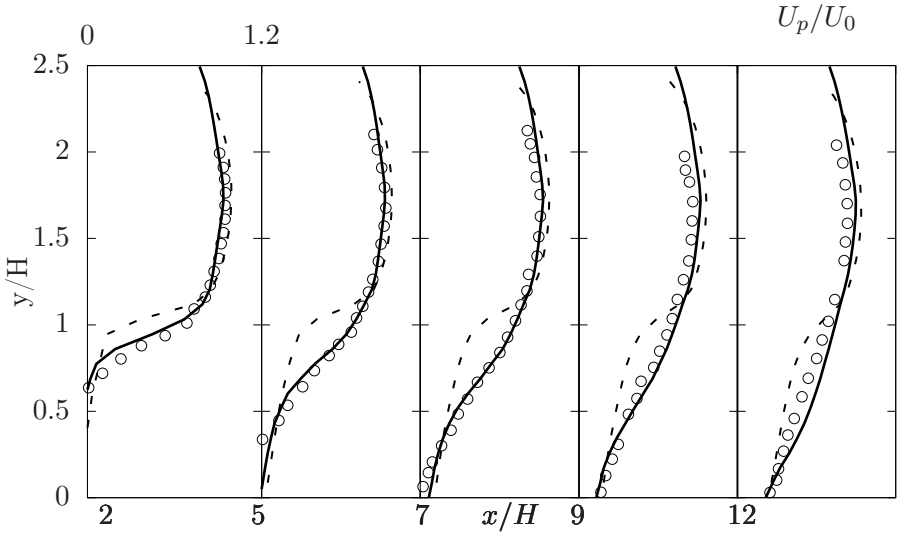

Figure 5: Stream-wise particle mean velocity for case 3. Solid line showing the RA-TFM and the dashed line showing the MPM. Data from Fessler and Eaton [19] with a mass-loading of 10%.

3.1. Mean particle stream-wise velocity

It is evident that across all three Figs. 3, 4 and 5 the prediction of the RA-TFM mean particle velocity profiles are in good agreement with the measured results. The

model captures the affects of varying St and mass loading on the mean velocity profile, especially in the recirculation region corresponding to locations (x/H = 2) and (x/H = 5). The MPM shows a marked difference around the step ($0.5 < y/H \leq 1$) as it does not include the correlated particle turbulent kinetic fluctuations. These stresses are responsible for forming the shear layer and leading to the production of turbulent viscosity.

All three Figs. 3, 4 and 5 show particle velocities with a flatter gradient across the depth of the pipe when compared to the fluid velocities, a feature that is not predicted by the MPM. This is attributed to the calculation of the particle phase viscosity. In the RA-TFM the calculation of the turbulent viscosity μ_{pt} appearing in the momentum equation is given by the $k_p - \varepsilon_p$ turbulence model, which accounts for the correlated turbulent kinetic particle fluctuations that are dominant due to the shear layer. In the MPM the viscosity is calculated directly from the granular temperature equation which relies on constitutive closures of thermal conductivity, shear viscosity and bulk viscosity [40]. As a result, a small value of both is predicted due to the dilute nature of the flow and this leads to a gross under-prediction of the particle viscosity. This then allows the momentum coupling term β to dominate in this region, which is why the mean velocity profiles tend to closely follow the fluid phase mean velocity profile.

Figs. 3 & 5 reveal the largest variation between the predicted mean particle velocity profiles in the shear layer. This is attributed to the particles St, which varies considerably over the shear layer as shown in both Figs ($y/H < 1$). When the particles St $\gg 1$ the particles tend to escape from the eddy they are in and ignore the influence of external eddies. This can either unite small eddies to create larger more energetic eddies or it can destroy large eddies which dissipate to smaller eddies. As a consequence of this for St $\gg 1$ we can expect the particle to take longer to react to the fluid. Therefore, when considering the shear layer the fluid response time, τ_f will be small in comparison with the channel flow resulting in a much higher local St. As a result the particle mean velocity profile does not show the sharp gradient across the ($y/H > 1$) and becomes much flatter.

Fig. 3 shows the case denoting both a high St (7.9) and a large mass loading (40%). It also corresponds to the largest over-prediction in the mean particle velocities at locations (x/H = 9 & 14) for the RA-TFM. These locations correspond to the redevelopment region which indicate that the energy in the particle phase is recovering too quickly in comparison to the measured data. This overestimation is difficult to explain as the predictions for case 3 with a large St are in good agreement. One potential source of error could be due to the distribution of the particles across the width of the pipe. As the particles pass the step they are redistributed

inhomogeneously (clustered) which reduces the slip velocity and as a result the drag. As the particles reach the redevelopment region they begin to redistribute homogeneously which increases the drag in this region. However neither model considers the effects of clustering in their drag model and are only representative of one particle. This can cause the observed over-estimation of the mean stream-wise velocities in the redevelopment region.

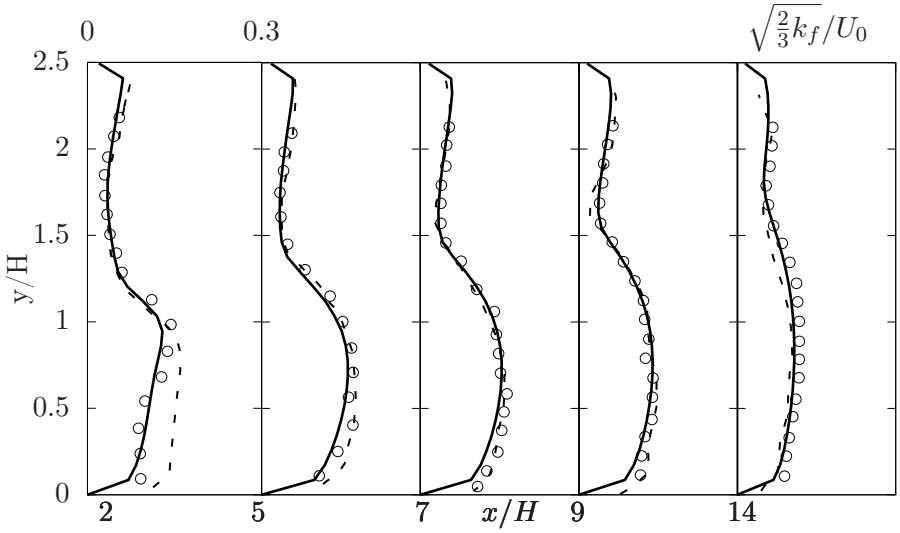

Figure 6: Fluid turbulent intensity for case 1. Solid line showing the RA-TFM and the dashed line showing the MPM. Data from Fessler and Eaton [19] with a mass-loading of 40%.

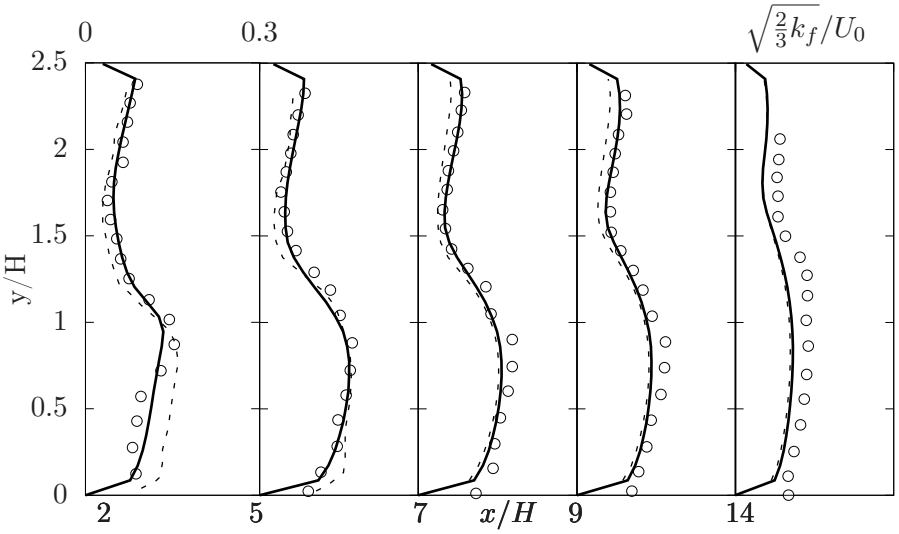

Figure 7: Fluid turbulent intensity for case 2. Solid line showing the RA-TFM and the dashed line showing the MPM. Data from Fessler and Eaton [19] with a mass-loading of 20%.

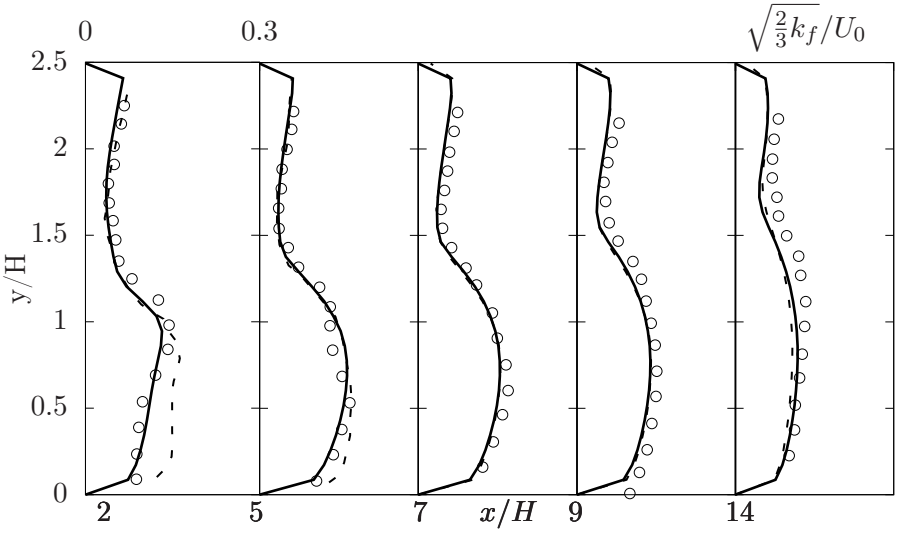

Figure 8: Fluid turbulent intensity for case 3. Solid line showing the RA-TFM and the dashed line showing the MPM. Data from Fessler and Eaton [19] with a mass-loading of 40%.

3.2. Fluid phase turbulence

As shown in the experiment of Fessler and Eaton [19], distinct turbulence attenuation was found for the two larger St cases (1 & 3). Over the region of (y/H $>$ 1)

extensive turbulence attenuation is shown across all five plots (corresponds to Fig. 9 in Fessler and Eaton [19]). Across locations (x/H = 2 & 5) there is attenuation across the range (y/H > 1) which shows that as mass loading is increased the turbulence is suppressed and below this range (y/H < 1) the turbulence is unaffected. This behaviour of turbulence attenuation was accurately predicted by the RA-TFM and the corresponding plots to those in [19] are Figs 6 & 8. The predictions are in good agreement with the experimental measurements. The turbulence attenuation for case 1 is as much as 35% showing a large reduction over the region of (y/H > 1) at (x/H = 2) on Fig. 8.

Below (y/H < 1) very little turbulence attenuation was observed, this corresponds to the shear layer and recirculation zone. From the simulations carried out, the particle turbulent quantities k_p & ε_p are produced and dissipated primarily near and at the wall and step (shear layer), with the contribution in the recirculation zone (y/H < 1) being several orders of magnitudes smaller. When considering the form of the coupling terms (see Section 2) it is evident why the turbulence attenuation is small in this region. This also follows from the lack of particles within the recirculation region due to the large St of all cases (St > 1) as the particles are not dragged into the eddy in the same way a particle of (St < 1) would.

The turbulence attenuation was accurately captured across all three particle classes for the RA-TFM. For the MPM an over-prediction of the fluid turbulent kinetic energy was observed. It was found that the form of the velocity correlation coupling term posed two major problems, the first being that as the term $k_{fp} = \sqrt{k_f \Theta_p}$ contains Θ_p directly the evolution of the term is adversely affected as the granular temperature equation evolves too quickly. This behaviour is recognised in two fluid model codes, and typically an upper limit is employed to constrain the initial stages of the solution to increase robustness.

Secondly, the source term of this form exists in both the k & ε transport equations, this leads to the formulation of the turbulent kinetic energy dissipation equation given by Elghobashi and Abou-Arab [16], which has been shown to yield incorrect behaviour [21], mainly as a consequence of failing to differentiate between the correlated and uncorrelated turbulent kinetic energy. Conversely, two coupling source terms are used in this work k_{fp} and ε_{fp} respectively. This allows the coupling of the turbulent kinetic energy k_i and dissipation ε_i equations of both phases to contain source terms that are of the same physical attribute i.e. particle turbulent kinetic energy and particle turbulence kinetic energy dissipation both contain separate coupling terms, which ensures conservation of energy between the two phases. In addition to this no numerical limiting was needed as the evolution of the granular temperature was controlled by the production of turbulent kinetic energy dissipation.

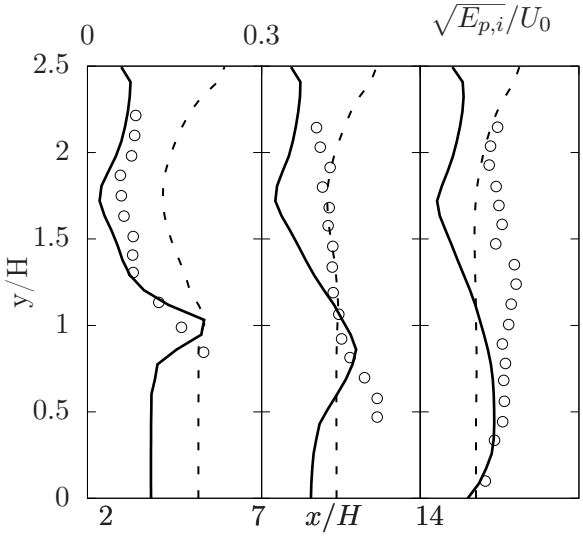

Figure 9: Particle turbulent intensity for case 1. Solid line showing the RA-TFM and the dashed line showing the MPM. Data from Fessler and Eaton [18] with a mass-loading of 40%.

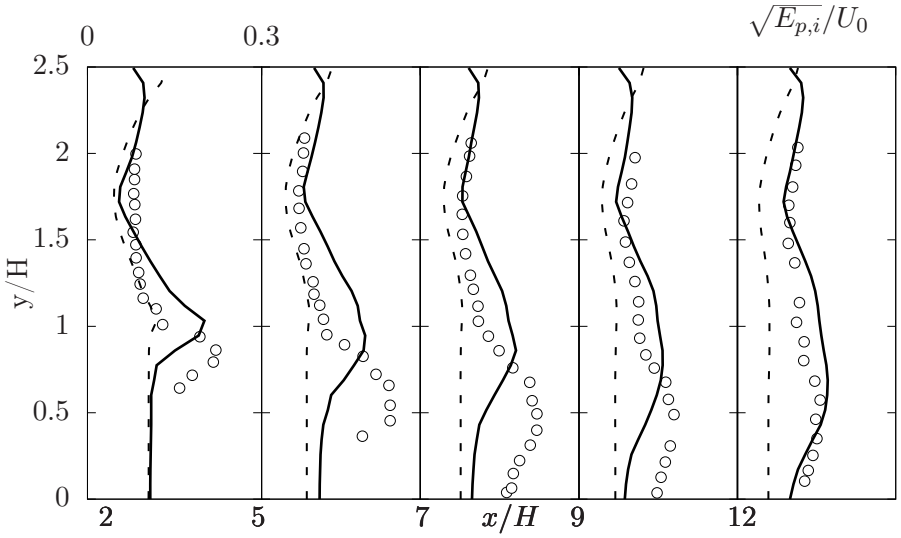

Figure 10: Particle turbulent intensity for case 3. Solid line showing the RA-TFM and the dashed line showing the MPM. Data from Fessler and Eaton [19] with a mass-loading of 10%.

3.3. Particle phase turbulence

From the experimental measurements it can be seen that the particles are being heavily influenced by the fluid phase's shear layer. This is true for both cases involving large St as shown in Fig 9 & 10. Looking at the results from the MPM the

prediction of the shear layer can not be seen across each location. Conversely, the RA-TFM is able to predict the presence of the shear layer and crucially convect it downstream. This feature is difficult to predict as the particles disperse and their fluctuating energy becomes more uniform across the profile. This result was almost exclusively attributed to the solution of the $k_p - \varepsilon_p$ transport equation.

As shown in Février et al. [20] the decomposition of the particle fluctuation energy into two components which reads, $\kappa_p = k_p + 3/2\Theta_p$ (following the notation of [21]) was needed when accounting for the particle's overall motion. Due to the step, turbulent scales at the integral scale are dominating the flow and as a result the large scale motions are the most relevant. This is reflected in the predictions of this model and highlighted when contrasted with the predictions of the MPM. Without the $k_p - \varepsilon_p$ transport model, the influence of the step is not captured and an under-prediction of the turbulent particle kinetic energy is seen. Table 3 shows the integral time scales associated with both flow regimes. This characteristic time scale associated with the particle turbulent kinetic energy enables the prediction of the shear layer and allows for the successful prediction of the predominant turbulent behaviour found in experiment across both Figs. 9 & 10.

Table 3: Table of integral time scales for each phase.

Flow regime	T_p	T_f
Channel flow centre line	0.04s	0.04s
Shear layer	4.09ms	5.12ms

In the MPM this definition of the particle-phase time scale is not present. The calculation of turbulent kinetic energy (granular temperature Θ_p) is heavily reliant on the constitutive relation of thermal conductivity, shear viscosity and bulk viscosity. As shown in both Figs. 9 & 10 the absence of the shear layer is demonstrated. The profiles are within the correct order of magnitude but the profile remains flat and largely unaffected by the step.

The $k_p - \varepsilon_p$ transport equation is modelled in an analogous manner to the single-phase $k - \varepsilon$ turbulence model using similar closure relations [41]. As a result some of the models well-known limitations are directly inherited. The Boussinesq approximation is one such limitation of RANS models of this form and introduces isotropy into the model; specifically the Reynolds stresses are assumed to be a scalar function of the mean velocity gradients. This introduction of isotropy has quite clear implications for the prediction of turbulent structures. The shear layer simulated in this studied is dominated by both the production term, Π_p and the turbulent dissipation

term, ε_p; the former is where the isotropy is introduced and that is why it is so influential. It has been shown by Simonin [44, 45] that the particle turbulence Reynold stresses are highly anisotropic and require transport equations for each term. This is a clear limitation of the current model and from the performance of the current RA-TFM an introduction of anisotropy for at least the particle phase is vital in an accurate prediction of the particle phase energy behaviour. Recently, Capecelatro et al. [7, 8] has derived a multiphase Reynolds-stress model which could fill this gap. Its application to a flow configuration similar to the one used in this work would be particularly interesting.

3.4. Particle wall boundary conditions

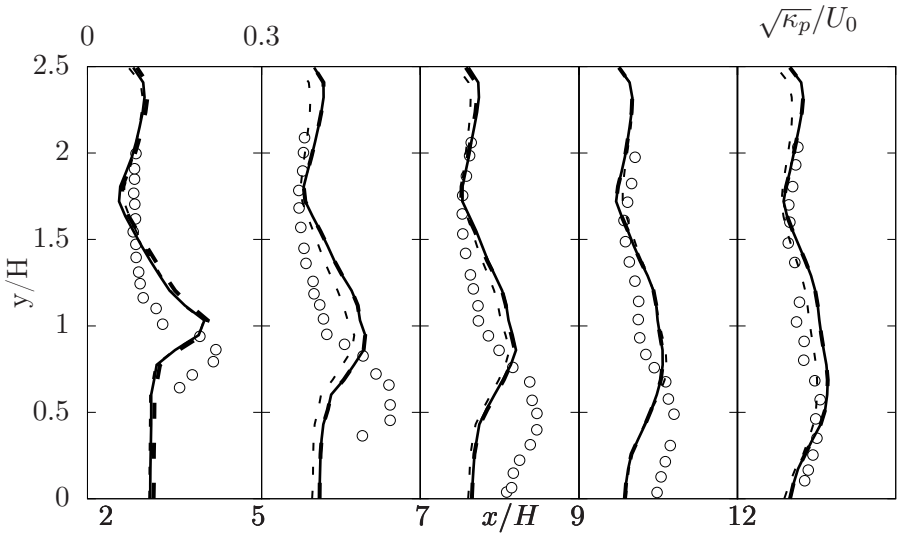

Figure 11: Particle turbulent intensity for case 3. Solid line showing the $\phi = 0.001$, thick dashed line showing $\phi = 0.01$ and the thin dashed line showing $\phi = 0$. Data from Fessler and Eaton [19] with a mass-loading of 10%.

As noted in Fessler and Eaton [19], the particles tend to conserve almost all their energy when interacting with the wall and consequently spend very little time interacting with it. As a consequence of this observation the specularity coefficient was varied from 0-0.01 in order to ascertain its effect on the numerical predictions.

Fig. 11 shows the particle turbulent intensity prediction of the RA-TFM with varying specularity coefficients. Immediately a general observation can be made; the particle phase wall boundary conditions have a relatively small impact on the prediction of particle fluctuation energy. This is to be expected as the particles

spend very little time interacting with the wall and the particle fluctuation energy is dominated by the production in the shear layer.

The biggest difference can be seen by comparing $\phi = 0$ with $\phi = 0.01 - 0.001$, and looking at locations (x/H = 5 - x/H = 12). The free slip condition exerts its influence on the prediction immediately downstream of the shear layer, this results in an underestimation in comparison with the larger ϕ values. When comparing this result with the experimental data it seems that the prediction lies closer to the measured values, this is seen most clearly at location (x/H = 5) across (y/H > 1) and across the whole profile at location (x/H = 12).

When comparing the near wall predictions of particle fluctuation energy it can be seen that there is a slight under-prediction when comparing $\phi = 0$ and $\phi = 0.01 - 0.001$. This is to be expected as a higher specularity coefficient will result in a higher value of particle fluctuation energy due to the production of mean particle shear. All three simulations under-predict the near wall behaviour, this result is attributed to the lack of particle phase fluctuation anisotropy, but put more explicitly the experimental observations show that the particle fluctuation energy is stretched in the wall-normal direction. This stretching continues up to the wall (at x/H = 7), the RA-TFM used in this work can not predict this behaviour due to the inherit assumptions made throughout.

A specularity coefficient value of 0.1 was tested but yielded unphysical results. [3, 61] also found that a low specularity coefficient was representative of high velocity, dilute fluid-particle flow. The unphysical results were due to the lowering of the slip velocity near the wall. The mean velocity profiles for the fluid and particle phase tend to converge as the no slip condition ($\phi = 1$) is approached. At the relatively high speed velocities used in this study this resulted in a gross overestimation of the particle fluctuation energy. An explanation for this behavior is as follows, the high specularity coefficient at the wall promotes "sticking" of the particles. As these particles are stuck at the wall and then released they begin to produce mean shear in the particle phase momentum equation. This shearing which is imposed by the boundary condition results in an overestimation of turbulence production resulting in excessively large values of the particle phase fluctuation energy.

3.5. RA-TFM discussion

Given the plethora of terms required to close the RA-TFM, a discussion of the relevant and negligible terms is warranted. The discussion is confined to the closure modelled terms with transport, convective and Laplacian terms omitted. We begin our discussion by focusing on the turbulent dispersion/drag/drift term which can be found in Eq. 2 & 4 of Section 2. Throughout the study this term remained

negligible and this was true for both the glass particles of case 1 & 2 and the copper particles of case 3. The reasons for this are two-fold: across the width of the pipe the gradient of the volume fraction remains small due to the uniformity imposed by gravity. This uniformity of the particle volume fraction across the pipe width of near identical conditions has also been reported by Vreman [54] & Yamamoto et al. [57]. This uniformity changes in the presence of the shear layer as there is a smaller particle volume fraction in the recirculating region than in the shear layer. This large particle volume fraction gradient is directly opposed by the increase of the St, as highlighted previously in Section 3.1 the St increases dramatically in the shear layer thus decreasing the amount of dispersion.

Next, the turbulent pressure term, which contains the term $2/3\rho_p\alpha_p k_p$, remains negligible throughout. This term arises due to compressibility effects which are expected to be high for large Mach numbers, which was not the case in this work. The covariance of the volume fraction and fluid pressure gradient remains very small throughout; this was to be expected as it represents the fluctuations in the buoyancy force. Due to the high density ratio, ρ_p/ρ_f the flow was not considered buoyancy driven and so this term was negligible.

The velocity-fluid-pressure-gradient covariance term was found to be negligible for glass particles but was vital in the successful prediction of the mean particle velocities of the copper particles. In fact, without this term the mean particle velocities were over-predicted by up to 10%. If we revisit this term it becomes clear as to why; the term takes the form $\alpha_p\rho_p\mathbf{g}$ (neglecting the constant density ratio) and when the particle volume fraction is present there is a static pressure gradient of the particles acting on the mean momentum of both the particle and fluid phase. This means that the mean slip velocity is affected by the imposed pressure gradient. In this work it resulted in a reduction of the mean particle velocities. Consequently, this term can not be neglected for particles with large densities or (put more generally) for large St.

For the multiphase turbulence modelling coupling terms found in Eq. 5, 6, 10 & 11, only the velocity correlation terms were found to be relevant for this flow. These terms are responsible for the turbulence attenuation, so it follows that they should remain. The volume-fraction-velocity correlation was found to be negligible due to the high density ratio used in this work, but for small density ratios this term may be relevant. The mean slip term was found to be non-negligible but its magnitude was not enough to affect the solution. Interestingly, in this work there was a large mean slip value near the wall which is where this term is expected to be at its largest. Due to the use of single-phase wall functions this behaviour may have been suppressed resulting in an underestimation.

Finally, a note on the limitations of the current approach. As shown in Fox [21] the hydrodynamic model (volume fraction. particle velocity and granular temperature) is derived from the mesoscale model i.e the Boltzmann equation, using a Chapman-Enskog expansion (shown in Garzó et al. [22]) in powers of Knudsen number. It is owing to this mathematical linearisation that the hydrodynamical model is not valid for large values of Knudsen number ($\mathrm{Kn} > 1$). The hydrodynamical model, as hinted at, is therefore most accurate for small values of Knudsen number ($\mathrm{Kn} \ll 1$), a feature of collisionally dominated flows (see Table 4 for Kn).

The flow regime used in this study is characterized as moderately dilute where collisions are expected. For the smallest mass loading (case 3), the Knudsen number was found to be ($\mathrm{Kn} < 10^{-4}$) across the pipe, whilst for higher mass loadings the Knudsen number was much lower. As this constraint is one across the whole domain this can not always be fulfilled. When considering a fluidised bed for example, the upper region of the chamber will not fulfill this criteria as no collisions are present as there are no particles. For this study the recirculating region posed a problem as only a small number of particles were present in the region. This meant that in this region the Knudsen number would fluctuate due to the vortex shedding and temporarily be $\mathcal{O}(1)$, compromising the validity of the solution. It was found that the value of granular temperature was relatively high which may have allowed for near equilibrium conditions thus satisfying the hydrodynamic constraint. Unfortunately, this type of constraint is unavoidable when employing a hydrodynamical description and this can not necessarily be fulfilled in every region of the flow. For a more flexible approach, kinetic-based equations can be formulated from moments (see [5, 32, 35, 39]).

4. Conclusions

The current work has investigated turbulent attenuation of moderately dilute flow in a vertically orientated backward-facing step using a Reynolds-Averaged Two-Fluid model. The RA-TFM model is implemented into OpenFOAM with the implementation procedure and the treatment of challenging terms provided. The model results are compared against benchmark experimental data and also against the model of Peirano and Leckner [40]. A summary of our findings are as follows:

1. Prediction of the mean particle velocities and both turbulence quantities (turbulent kinetic energy of the fluid and particles) were in good agreement with the benchmark experimental data.
2. The inclusion of the correlated k_p and uncorrelated Θ_p particle motion was crucial in accurately predicting the behaviour of the turbulent shear layer. This was further highlighted when compared to the turbulent particle kinetic energy predictions from the modified Peirano model.
3. The form of the velocity correlation coupling terms, i.e. separate coupling terms for turbulent kinetic energy and turbulent kinetic energy dissipation, resulted in a successful prediction of turbulence attenuation.
4. A specularity coefficient value of 0.001 was found to be representative of the particle-wall behaviour in this study. Changes in the specularity coefficient ($\phi < 0.01$) had very little effect on the particle fluctuation energy prediction.
5. It has been shown that the behaviour of the particles interacting in a shear layer is highly anisotropic. The current predictions of this behaviour are limited due to the reliance on the Boussinesq approximation which introduces isotropy into the model.

Nomenclature

U_0	centreline velocity, [ms^{-1}]
C_D	drag coefficient, [−]
A_i	diagonal coefficients of the matrix
g	gravity, [ms^{-2}]
$\mathbf{n}$	unit vector normal to the wall, [−]
Re_p	particle Reynolds number, [−]
d_p	particle diameter, [m]
$\mathbf{u}_i$	velocity, [ms^{-1}]
$\mathbf{u}_w$	wall velocity, [ms^{-1}]
$\mathbf{u}_{p,w}$	particle slip velocity parallel to the wall, [ms^{-1}]
$\mathbf{u}_p''$	particle velocity fluctuation w.r.t PA velocity, [ms^{-1}]
$\mathbf{u}_{p,i}''^2$	particle Reynolds stress component in direction i, [ms^{-1}]
$\mathbf{u}_f'''$	fluid velocity fluctuation w.r.t PA velocity, [ms^{-1}]
h	pipe width, [m]
p_i	pressure, [Pa]
g_0	radial distribution coefficient, [−]
H	step height, [m]
t	time, [s]
k_i	turbulent kinetic energy, [m^{2}s^{-2}]

Greek letters

α_i	volume fraction, [−]
$\alpha_{p,max}$	maximum particle volume fraction, [−]
β	momentum exchange coefficient, [$\mathrm{kgm^{-3}s^{-1}}$]
ε_i	turbulent kinetic energy dissipation, [$\mathrm{m^2s^{-3}}$]
Θ_p	granular temperature, [$\mathrm{m^2s^{-2}}$]
κ_p	particle fluctuation energy, [$\mathrm{m^2s^{-2}}$]
$\kappa_{\Theta s}$	diffusion coefficient for granular energy, [$\mathrm{kgm^{-1}s^{-1}}$]
μ_i	shear viscosity, [$\mathrm{kgm^{-1}s^{-1}}$]
$\mu_{i,t}$	turbulent shear viscosity, [$\mathrm{kgm^{-1}s^{-1}}$]
ν_i	kinematic viscosity, [$\mathrm{m^2s^{-1}}$]
$\nu_{i,t}$	turbulent kinematic viscosity, [$\mathrm{m^2s^{-1}}$]
ρ_i	density, [$\mathrm{kgm^{-3}}$]
$\overline{\boldsymbol{\sigma}}_f$	fluid phase stress tensor,[$\mathrm{kgm^{-1}s^{-2}}$]
$\overline{\boldsymbol{\sigma}}_p$	particle phase stress tensor, [$\mathrm{kgm^{-1}s^{-2}}$]
τ_d	particle relaxation time, [s]

Subscripts

1	RA-TFM
2	MPM
f	fluid
i	general index
p	particle
x	x direction
y	y direction
z	z direction

Superscripts

$''$	PA particle velocity fluctuation
$'''$	PA fluid velocity fluctuation

Special notation

$\langle\cdot\rangle$	Reynolds averaging operator
$\langle\cdot\rangle_i$	phase averaging operator associated with phase i

Table 4: Model characteristics.

$$\beta = \frac{\rho_p \alpha_p}{\tau_d} = \frac{3}{4} \frac{\alpha_p \alpha_f \rho_f \mathbf{u}_r}{d_p} C_d$$

$$\mathrm{C}_d = \begin{cases} \frac{24}{Re_p} \left[1 + 0.15 Re_p^{0.287} \right] & \text{if } Re_p < 1000 \\ 0.44 & \text{if } Re_p \geq 1000 \end{cases}$$

$$Re_p = \frac{\rho_f d_p |\mathbf{u}_p - \mathbf{u}_f|}{\mu_f}$$

$$\mathrm{E}_{p,1} \equiv \kappa_p = k_p + 3/2\Theta_p$$

$$\mathrm{E}_{p,2} \equiv \kappa_p = 3/2\Theta_p$$

$$\tau_f \equiv T_f = k_f / \varepsilon_f$$

$$\mathrm{St} = \tau_d / \tau_f$$

$$\mathrm{T}_p = \frac{k_p}{\varepsilon_p}$$

$$\mathrm{Kn} = \frac{\sqrt{\pi} d_p}{12 \alpha_p g_0 L}$$

$$\chi = \frac{\alpha_p \rho_p}{\alpha_f \rho_f}$$

$$\mathrm{e} = 0.9$$

Table 5: Definition of variables.

$$\kappa_p = k_p + 1.5\Theta_p$$

$$\mu_f = \rho_f \nu_f$$

$$\mu_{ft} = \alpha_f \rho_f \nu_{ft} = \alpha_f \rho_f C_{f\mu} \frac{k_f^2}{\varepsilon_f}$$

$$\mu_p = \alpha_p \rho_p \nu_p = \frac{2\mu_{p_{dil}}}{(1+e)g_0}\Big[1 + \frac{4}{5}(1+e)g_0\alpha_p\Big]^2 + \frac{4}{5}\alpha_p^2 \rho_p d_p g_0 (1+e)\Big(\frac{\Theta_p}{\pi}\Big)^{1/2}$$

$$\mu_{p_{dil}} = \frac{5\sqrt{\pi}}{96}\rho_p d_p \Theta_p^{1/2}$$

$$\mu_{pt} = \alpha_p \rho_p \nu_{pt} = \alpha_p \rho_p C_{p\mu} \frac{k_p^2}{\varepsilon_p}$$

$$\mathrm{p}_p = \rho_p \alpha_p \Theta_p + 2(1+e)\rho_p \alpha_p^2 g_0 \Theta_p$$

$$\gamma = \frac{12(1-e^2)g_o}{\sqrt{\pi} d_p}\alpha_p^2 \rho_p \Theta_p^{3/2}$$

$$\kappa_\Theta = \frac{2}{(1+e)g_0}\Big[1 + \frac{6}{5}(1+e)g_0\alpha_p\Big]^2 \kappa_{\Theta,dil} + 2\alpha_p^2 \rho_p d_p g_0 (1+e)\Big(\frac{\Theta_p}{\pi}\Big)^{\frac{1}{2}}$$

$$\kappa_{\Theta,dil} = \frac{75}{384}\sqrt{\pi}\rho_p d_p \Theta_p^{1/2}$$

$$g_0 = \Big[1 - \Big(\frac{\alpha_p}{\alpha_{p,max}}\Big)^{\frac{1}{3}}\Big]^{-1}$$

$$\overline{\mathbf{S}}_\mathbf{p} = \frac{1}{2}[\nabla \mathbf{u}_p + (\nabla \mathbf{u}_p)^T] - \frac{1}{3}\nabla \cdot \mathbf{u}_p \mathbf{I}$$

$$\overline{\mathbf{S}}_\mathbf{f} = \frac{1}{2}[\nabla \mathbf{u}_f + (\nabla \mathbf{u}_f)^T] - \frac{1}{3}\nabla \cdot \mathbf{u}_f \mathbf{I}$$

$$k_{fp} = \beta_k \sqrt{k_f k_p}$$

$$\varepsilon_{fp} = \beta_\varepsilon \sqrt{\varepsilon_f \varepsilon_p}$$

Table 6: Definition of phase-averaged variables.

$$\alpha_p = \langle \alpha_p \rangle$$

$$\alpha_f = \langle \alpha_f \rangle$$

$$\mathbf{u}_p = \langle \mathbf{u} \rangle_p$$

$$\mathbf{u}_f = \langle \mathbf{u} \rangle_f$$

$$\Theta_p = \langle \Theta \rangle_p$$

$$k_p = \frac{1}{2} \langle \mathbf{u}_p'' \cdot \mathbf{u}_p'' \rangle_p$$

$$k_f = \frac{1}{2} \langle \mathbf{u}_f''' \cdot \mathbf{u}_f''' \rangle_f$$

$$\varepsilon_p = \frac{1}{\rho_p \alpha_p} \langle \bar{\boldsymbol{\sigma}}_p : \nabla \mathbf{u}_p'' \rangle$$

$$\varepsilon_f = \frac{1}{\rho_f \alpha_f} \langle \bar{\boldsymbol{\sigma}}_f : \nabla \mathbf{u}_f''' \rangle$$

$$\overline{\boldsymbol{\sigma}}_p = \mu_p [\nabla \mathbf{u}_p + (\nabla \mathbf{u}_p)^T] - \frac{1}{3} \mu_p \nabla \cdot \mathbf{u}_p \mathbf{I}$$

$$\overline{\boldsymbol{\sigma}}_f = \mu_f [\nabla \mathbf{u}_f + (\nabla \mathbf{u}_f)^T] - \frac{1}{3} \mu_f \nabla \cdot \mathbf{u}_f \mathbf{I}$$

$$\mathbf{u}_p'' = \mathbf{u}_p - \langle \mathbf{u}_p \rangle_p$$

$$\mathbf{q}_\Theta = \langle \mathbf{q}_\Theta \rangle_p = \frac{\kappa_\Theta}{\alpha_p \rho_p} \nabla \Theta_p$$

$$\mathbf{u}_f''' = \mathbf{u}_f - \langle \mathbf{u}_f \rangle_f$$

$$\langle \mathbf{u}_p \rangle_p = \langle \alpha_p \mathbf{u}_p \rangle / \langle \alpha_p \rangle$$

$$\langle \mathbf{u}_f \rangle_f = \langle \alpha_f \mathbf{u}_f \rangle / \langle \alpha_f \rangle$$

$$\mathbf{u}_p'' \mathbf{u}_p'' = \langle \mathbf{u}_p'' \mathbf{u}_p'' \rangle_p$$

5. Appendix

Here the equations used in the MPM are presented. A full explanation of the equations can be found in Peirano and Leckner [40]. The modification of the model comes from the type of closure for the particle-fluid covariance in which the isotropic model of Sinclair and Mallo [46] is used.
The continuity equations for each phase read:

$$\frac{\partial \alpha_p \rho_p}{\partial t} + \nabla \cdot \alpha_p \rho_p \mathbf{u}_p = 0 \tag{42}$$

$$\frac{\partial \alpha_f \rho_f}{\partial t} + \nabla \cdot \alpha_f \rho_f \mathbf{u}_f = 0 \tag{43}$$

The momentum balance equation for each phase:

$$\frac{\partial \alpha_p \rho_p \mathbf{u}_p}{\partial t} + \nabla \cdot \alpha_p \rho_p \mathbf{u}_p \mathbf{u}_p = \alpha_p \nabla \cdot \tau_p - \alpha_p \nabla p_f - \nabla p_p + \beta(\mathbf{u}_f - \mathbf{u}_p) + \alpha_p \rho_p \mathbf{g} \tag{44}$$

$$\frac{\partial \alpha_f \rho_f \mathbf{u}_f}{\partial t} + \nabla \cdot \alpha_f \rho_f \mathbf{u}_f \mathbf{u}_f = \alpha_f \nabla \cdot \tau_f - \alpha_f \nabla p_f - \beta(\mathbf{u}_p - \mathbf{u}_f) + \alpha_f \rho_f \mathbf{g} \tag{45}$$

5.1. Kinetic Theory of Granular Flow

Following the kinetic theory of granular flow the closure of the particle pressure, shear and bulk viscosities can be provided. The granular temperature Θ_p is introduced as a measure of the particle velocity fluctuations [23].

$$\Theta_p = \frac{1}{3}\mathbf{u}_p''^2 \tag{46}$$

where $\mathbf{u}_p''$ is the particle fluctuation velocity. A balance equation is introduced for the granular energy ($\frac{3}{2}\Theta_p$) to satisfy the continuity and momentum balance for both phases. The fluctuation energy conservation for the particles is then given as:

$$\frac{3}{2}\Big[\frac{\partial \alpha_p \rho_p \Theta_p}{\partial t} + \nabla \cdot \alpha_p \rho_p \Theta_p \mathbf{u}_p\Big] = (p_p \bar{\bar{I}} + \bar{\bar{\tau}}) : \nabla \mathbf{u}_p + \nabla \cdot \kappa \nabla \Theta_p - \gamma_p + J_{vis} + J_{slip} \tag{47}$$

where the first term on the RHS is the fluctuation energy created by the shearing in the particle phase. The second term is associated with the diffusion of fluctuating energy, the third term is responsible for the dissipation due to inelastic collisions.

Finally, J_s is either dissipation of granular temperature due to viscous damping and/or creation of granular temperature from the slip between the fluid and particles. Both terms can be written more intuitively to read:

$$J_{vis} + J_{slip} = \beta(\mathbf{u}_p''\mathbf{u}_p'' - \mathbf{u}_p''\mathbf{u}_f''') \tag{48}$$

The first term can be modeled as $3\Theta_p$ according to Gidaspow [23] and the last term can be modeled as k_{pf}.

5.2. Turbulence modelling

The transport equations for the fluid phases turbulence model $k_f - \varepsilon_f$ reads as follows:

$$\frac{\partial \alpha_f \rho_f k_f}{\partial t} + \nabla \cdot \alpha_f \rho_f k_f \mathbf{u}_f = \nabla \cdot \alpha_f \rho_f \nu_t \nabla k_f + \alpha_f G - \alpha_f \rho_f \varepsilon_f + \Pi_{kf} \tag{49}$$

$$\frac{\partial \alpha_f \rho_f \varepsilon_f}{\partial t} + \nabla \cdot \alpha_f \rho_f \varepsilon_f \mathbf{u}_f = \nabla \cdot \alpha_f \rho_f \nu_t \nabla \varepsilon_f + \frac{\varepsilon_f}{k_f}\Big[C_1 \alpha_f G - C_2 \alpha_f \rho_f \varepsilon_f + C_3 \Pi_{kf}\Big] \tag{50}$$

Where G is the production of the turbulent kinetic energy, which is expressed as follows:

$$G = 2\nu\rho_f\Big(\overline{\mathbf{S}}_\mathbf{f} : \overline{\mathbf{S}}_\mathbf{f} - \frac{2}{3} tr(\overline{\mathbf{S}}_\mathbf{f})^2 \cdot \mathbf{I}\Big) + \frac{2}{3}\rho_f k_f \nabla \cdot (\mathbf{u}_f \mathbf{I}) \tag{51}$$

The term Π_{kf} accounts for turbulence modulation from particles and represents the velocity fluctuation correlation of each phase,

$$\Pi_{kf} = -\beta(2k_f - k_{pf} - \mathbf{u}_r \mathbf{u}_d) \tag{52}$$

The term $\mathbf{u}_d$ accounts for turbulence dispersion and is also known as the drift velocity. Here it is given from the formulation of [44].

$$\mathbf{u}_d = -D_{sf}\Big(\frac{1}{\alpha_p}\nabla\alpha_p - \frac{1}{\alpha_f}\nabla\alpha_f\Big) \tag{53}$$

The fluid-particle covariance term is given by Sinclair and Mallo [46] and is also termed an isotropic model.

$$k_{pf} = c_{pf}\sqrt{k_f \Theta_p} \tag{54}$$

6. Bibliography

[1] Anderson, T. B. and Jackson, R. (1967). Fluid mechanical description of fluidized beds: Equations of Motion. *Industrial and Engineering Chemistry Fundamentals*, 6(4):527–539.

[2] Benavides, A. and van Wachem, B. (2008). Numerical simulation and validation of dilute turbulent gas-particle flow with inelastic collisions and turbulence modulation. *Powder Technology*, 182:294–306.

[3] Benyahia, S., Syamlal, M., and O'Brien, T. J. (2005). Evaluation of boundary conditions used to model dilute, turbulent gas/solids flows in a pipe. *Powder Technology*, 156(2):62 – 72. Particle Technology Forum Special Issue.

[4] Borée, J. and Caraman, N. (2005). Dilute bidispersed tube flow: Role of interclass collisions at increased loadings. *Physics of Fluids*, 17(5):055108.

[5] Buffo, A., Vanni, M., and Marchisio, D. L. (2016). On the implementation of moment transport equations in OpenFOAM : Boundedness and realizability. *International Journal of Multiphase Flow*, 85:223 – 235.

[6] Capecelatro, J., Desjardins, O., and Fox, R. O. (2015). On fluid-particle dynamics in fully developed cluster-induced turbulence. *Journal of Fluid Mechanics*, 780:578–635.

[7] Capecelatro, J., Desjardins, O., and Fox, R. O. (2016a). Strongly coupled fluid-particle flows in vertical channels. I. Reynolds-averaged two-phase turbulence statistics. *Physics of Fluids*, 28(3).

[8] Capecelatro, J., Desjardins, O., and Fox, R. O. (2016b). Strongly coupled fluid-particle flows in vertical channels. II. Turbulence modeling. *Physics of Fluids*, 28(3).

[9] Caraman, N., Borée, J., and Simonin, O. (2003). Effect of collisions on the dispersed phase fluctuation in a dilute tube flow: Experimental and theoretical analysis. *Physics of Fluids*, 15(12):3602–3612.

[10] Chan, C. K., Zhang, H. Q., and Lau, K. S. (2001). Numerical simulation of gas-particle flows behind a backward-facing step using an improved stochastic separated flow model. *Computational Mechanics*, 27(5):412–417.

[11] Dasgupta, S., Jackson, R., and Sundaresan, S. (1994). Turbulent gas-particle flow in vertical risers. *AIChE Journal*, 40(2):215–228.

[12] Dasgupta, S., Jackson, R., and Sundaresan, S. (1998). Gas-particle flow in vertical pipes with high mass loading of particles. *Powder Technology*, 96(1):6 – 23.

[13] Drew, D. A. and Lahey, R. T. (1993). *In particulate Two-phase Flow.* Butterworth-Heinemann, Boston.

[14] Elghobashi, S. (1994). On predicting particle-laden turbulent flows. *Applied Scientific Research*, 52(4):309–329.

[15] Elghobashi, S. and Truesdell, G. C. (2006). Direct simulation of particle dispersion in a decaying isotropic turbulence. *Journal of Fluid Mechanics*, 242(-1):655.

[16] Elghobashi, S. E. and Abou-Arab, T. W. (1983). A two-equation turbulence model for two-phase flows. *Physics of Fluids*, 26(4):931.

[17] Ferziger, J. H. and Perić, M. (2002). *Computational Methods for Fluid Dynamics.* Springer.

[18] Fessler, J. R. and Eaton, J. K. (1995). Particle-turbulence interaction in a backward-facing step flow. *Rep. MD-70*, 394(1995):97–117.

[19] Fessler, J. R. and Eaton, J. K. (1999). Turbulence modification by particles in a backward-facing step flow. *Journal of Fluid Mechanics*, 394(1999):97–117.

[20] Février, P., Simonin, O., and Squires, K. D. (2005). Partitioning of particle velocities in gas solid turbulent flows into a continuous field and a spatially uncorrelated random distribution: theoretical formalism and numerical study. *Journal of Fluid Mechanics*, 533:1–46.

[21] Fox, R. O. (2014). On multiphase turbulence models for collisional fluid-particle flows. *Journal of Fluid Mechanics*, 742:368–424.

[22] Garzó, V., Tenneti, S., Subramaniam, S., and Hrenya, C. M. (2012). Enskog kinetic theory for monodisperse gas-solid flows. *Journal of Fluid Mechanics*, 712:129–168.

[23] Gidaspow, D. (1994). *Multiphase flow and fluidization.* Academic Press.

[24] Gore, R. and Crowe, C. (1989). Effect of particle size on modulating turbulent intensity. *International Journal of Multiphase Flow*, 15(2):279 – 285.

[25] Helland, E., Occelli, R., and Tadrist, L. (2002). Computational study of fluctuating motions and cluster structures in gasâĂŞparticle flows. *International Journal of Multiphase Flow*, 28(2):199 – 223.

[26] Hetsroni, G. (1989). Particles-turbulence interaction. *International Journal of Multiphase Flow*, 15(5):735 – 746.

[27] Hrenya, C. and Sinclair, J. (1997). Effects of particle-phase turbulence in gas-solid flows. *AIChE Journal*, 43(4):853–869.

[28] Ishii, M. (1975). Thermo-fluid dynamic theory of two-phase flow. *NASA STI/Recon Technical Report A*, 75.

[29] Issa, R. I. (1986). Solution of the implicitly discretised fluid flow equations by operator-splitting. *Journal of Computational Physics*, 62(1):40–65.

[30] Jasak, H. (1996). Error Analysis and Estimation for the Finite Volume Method with Applications to Fluid Flows. *PhD Thesis,*, Imperial College London(June).

[31] Johnson, P. C. and Jackson, R. (1987). Friction-collisional constitutive relations for granular materials, with application to plane shearing. *Journal of Fluid Mechanics*.

[32] Kong, B. and Fox, R. O. (2017). A solution algorithm for fluid-particle flows across all flow regimes. *Journal of Computational Physics*, 344:575 – 594.

[33] Kulick, J., Fessler, J. R., and Eaton, J. R. (1994). Particle response and turbulence modification in fully developed channel flow. *Journal of Fluid Mechanics*, 277:109–134.

[34] Liu, X. and Xu, X. (2009). Modelling of dense gas-particle flow in a circulating fluidized bed by distinct cluster method (dcm). *Powder Technology*, 195(3):235 – 244.

[35] Marchisio, D. L. and Fox, R. O. (2013). *Computational Models for Polydisperse Particulate and Multiphase Systems*. Cambridge Series in Chemical Engineering. Cambridge University Press.

[36] Mohanarangam, K. and Tu, J. Y. (2007). Two-fluid model for particle-turbulence interaction in a backward-facing step. *AIChE Journal*, 53(9):2254–2264.

[37] Moukalled, F., Mangani, L., and Darwish, M. (2015). *The Finite Volume Method in Computational Fluid Dynamics: An Advanced Introduction with OpenFOAM and Matlab*. Springer Publishing Company, Incorporated, 1st edition.

[38] Mukin, R. V. and Zaichik, L. I. (2012). Nonlinear algebraic Reynolds stress model for two-phase turbulent flows laden with small heavy particles. *International Journal of Heat and Fluid Flow*, 33(1):81–91.

[39] Passalacqua, A., Fox, R., Garg, R., and Subramaniam, S. (2010). A fully coupled quadrature-based moment method for dilute to moderately dilute fluid-particle flows. *Chemical Engineering Science*, 65(7):2267 – 2283. International Symposium on Mathematics in Chemical Kinetics and Engineering.

[40] Peirano, E. and Leckner, B. (1998). Fundamentals of turbulent gas-solid flows applied to circulating fluidized bed combustion. *Doktorsavhandlingar vid Chalmers Tekniska Hogskola*, 24(1381):259–296.

[41] Pope, S. B. (2011). *Turbulent flows*. Cambridge Univ. Press, Cambridge.

[42] Rhie, C. M. and Chow, W. L. (1983). A numerical study of the turbulent flow past an isolated airfoil with trailing edge separation. *AIAA J.*, pages 1525–1532.

[43] Rusche, H. (2002). Computational Fluid Dynamics of Dispersed Two-Phase Flows at High Phase Fractions. *PhD Thesis*, (December).

[44] Simonin, O. (1991). Second-moment prediction of dispersed phase turbulence in particle-laden flows. *Proceedings of 8th International Symposium on Turbulent Shear Flows*, 1(4):741–746.

[45] Simonin, O. (1996). Continuum modeling of dispersed turbulent two-phase flows. Part 1: General model description. *Combustion and Turbulence in Two-phase Flows*.

[46] Sinclair, J. and Mallo, T. (1998). Describing particle-turbulence interaction in a two-fluid modeling framework. *Proceedings of FEDSM'98: ASME Fluids Engineering Division Summer Meeting*, 4:7–14.

[47] Soo, S. L. (1990). *Multiphase Fluid Dynamics*. Science Press, Gower Technical, New York.

[48] Syamlal, M. and O'Brien, T. J. (1989). Computer simulation of bubbles in a fluidized bed. *AIChE Symposium Series*, 85(270):22–31.

[49] Tanaka, T., Yonemura, S., Kiribayashi, K., and Tsuji, Y. (1996). Cluster formation and particle-induced instability in gas-solid flows predicted by the dsmc method. *JSME International Journal Series B*, 39(2):239–245.

[50] Tsuji, Y. and Morikawa, Y. (1984). LDV measurements of an air-solid two-phase flow in a vertical pipe. *Journal of Fluid Mechanics*, 120:385–409.

[51] Van Wachem, B. G. M., Schouten, J. C., Van den Bleek, C. M., Krishna, R., and Sinclair, J. L. (2001). Comparative analysis of CFD models of dense gas-solid systems. *AIChE Journal*, (5).

[52] Viollet, P. L. and Simonin, O. (1994). Modelling dispersed two-phase flows: Closure, validation and software development. *Appl. Mech. Rev.*, 47:s80–s84.

[53] Vreman, A. W. (2007). Turbulence characteristics of particle-laden pipe flow. *Journal of Fluid Mechanics*, 584:235–279.

[54] Vreman, A. W. (2015). Turbulence attenuation in particle-laden flow in smooth and rough channels. *Journal of Fluid Mechanics*, 773:103–136.

[55] Weller, H. (2002). Derivation, modelling and solution of the conditionally averaged two-phase flow equations. *Tech.Rep.OpenCFD Ltd.*

[56] Weller, H. G., Tabor, G., Jasak, H., and Fureby, C. (1998). A tensorial approach to computational continuum mechanics using object-oriented techniques. *Computers in Physics*, 12(6):620–631.

[57] Yamamoto, Y., Potthoff, M., Tanaka, T., Kajishima, T., and Tsuji, Y. (2001). Large-eddy simulation of turbulent gas-particle flow in a vertical channel: effect of considering inter-particle collisions. *Journal of Fluid Mechanics*, 442:303–334.

[58] Yu, K., Lau, K., and Chan, C. (2004). Numerical simulation of gas-particle flow in a single-side backward-facing step flow. *Journal of Computational and Applied Mathematics*, 163(1):319 – 331. Proceedings of the International Symposium on Computational Mathematics and Applications.

[59] Zalesak, S. T. (1979). Fully multidimensional flux-corrected transport algorithms for fluids. *Journal of Computational Physics*, 31(3):335–362.

[60] Zheng, Y., Wan, X., Qian, Z., Wei, F., and Jin, Y. (2001). Numerical simulation of the gas-particle turbulent flow in riser reactor based on k-ϵ-kp-ϵp-θ two-fluid model. *Chemical Engineering Science*, 56(24):6813–6822.

[61] Zhou, X., Gao, J., Xu, C., and Lan, X. (2013). Effect of wall boundary condition on CFD simulation of CFB risers. *Particuology*, 11(5):556 – 565.